

1 **Article manuscript (Main text 3,989 words)**

2 **Title**

3 **Differential involvement of LUBAC-mediated linear ubiquitination in intestinal epithelial**
4 **cells and macrophages during intestinal inflammation**

5
6 **Running title (68 characters)**

7 Linear ubiquitination in intestinal epithelial cells and macrophages

8
9 **Authors and affiliations**

10 **Yusuke Sakamoto^{1,2}, Katsuhiko Sasaki¹, Mayuki Omatsu³, Kensuke Hamada³, Yuki**
11 **Nakanishi³, Yoshiro Itatani², Kenji Kawada², Kazutaka Obama², Hiroshi Seno³ and**
12 **Kazuhiro Iwai^{1*}**

13
14 ¹Department of Molecular and Cellular Physiology, Graduate School of Medicine, Kyoto
15 University, Kyoto, Japan.

16 ²Department of Surgery, Graduate School of Medicine, Kyoto University, Kyoto, Japan.

17 ³Department of Gastroenterology and Hepatology, Graduate School of Medicine, Kyoto
18 University, Kyoto, Japan.

19
20 ***Correspondence to**

21 Kazuhiro Iwai

22 Department of Molecular and Cellular Physiology, Graduate School of Medicine, Kyoto
23 University, Yoshida-Konoe-cho, Sakyo-ku, Kyoto 606-8501, Japan

24 Phone: +81-75-753-4671; Fax: +81-75-753-4676

25 E-mail: kiwai@mcp.med.kyoto-u.ac.jp

26

27 **Conflict of interest statement**

28 The authors declare no competing financial interests.

29 **Abstract (284 words)**

30 **Disruption of the intestinal epithelial barrier and dysregulation of macrophages are major**
31 **factors contributing to the pathogenesis of inflammatory bowel diseases (IBDs).**
32 **Activation of NF- κ B and cell death are involved in maintaining intestinal homeostasis in**
33 **a cell type-dependent manner. Although both are regulated by linear ubiquitin chain**
34 **assembly complex (LUBAC)-mediated linear ubiquitination, the physiological relevance**
35 **of linear ubiquitination to intestinal inflammation remains unexplored. Here, we used two**
36 **experimental mouse models of IBD (intraperitoneal LPS and oral dextran sodium**
37 **sulphate (DSS) administration) to examine the role of linear ubiquitination in intestinal**
38 **epithelial cells (IECs) and macrophages during intestinal inflammation. We did this by**
39 **deleting the linear ubiquitination activity of LUBAC specifically from IECs or**
40 **macrophages. Upon LPS administration, loss of ligase activity in IECs induced mucosal**
41 **inflammation and augmented IEC death. LPS-mediated death of LUBAC-defective IECs**
42 **was triggered by TNF. IEC death was rescued by an anti-TNF antibody, and TNF (but not**
43 **LPS) induced apoptosis of organoids derived from LUBAC-defective IECs. However,**
44 **augmented TNF-mediated IEC death did not overtly affect the severity of colitis after DSS**
45 **administration. By contrast, defective LUBAC ligase activity in macrophages ameliorated**
46 **DSS-induced colitis by attenuating both infiltration of macrophages and expression of**
47 **inflammatory cytokines. Decreased production of macrophage chemoattractant MCP-**
48 **1/CCL2, as well as pro-inflammatory IL-6 and TNF, occurred through impaired**
49 **activation of NF- κ B and ERK via loss of ligase activity in macrophages. Taken together,**
50 **these results indicate that both intraperitoneal LPS and oral DSS administrations are**
51 **beneficial for evaluating epithelial integrity under inflammatory conditions, as well as**
52 **macrophage functions in the event of an epithelial barrier breach. The data clarify the**
53 **cell-specific roles of linear ubiquitination as a critical regulator of TNF-mediated**

54 **epithelial integrity and macrophage pro-inflammatory responses during intestinal**
55 **inflammation.**

56

57 **Keywords (10)**

58 **LUBAC; linear ubiquitination; NF- κ B; cell death; intestinal epithelial cells;**

59 **macrophages; DSS; LPS; IBD; intestinal inflammation**

60 **Introduction**

61 Inflammatory bowel diseases (IBDs), including Crohn's disease and ulcerative colitis, are
62 characterized by chronic and relapsing inflammation in the gut; these conditions affect 6.8
63 million individuals worldwide [1]. Although the pathogenesis of IBDs is thought to involve
64 genetic, environmental, microbial, epithelial, and immune factors, the pathophysiology still
65 remains unclear, resulting in inadequate responses to currently available treatments [2-4].
66 Recent [studies](#) show that the innate immune system, including epithelial barrier function and
67 microbial sensing by macrophages, also plays an important role in the pathogenesis of IBDs,
68 as do adaptive immune responses such as T cell-derived inflammatory cytokines [5-7].

69 Intestinal epithelial cells (IECs) maintain intestinal homeostasis by forming a physical and
70 chemical barrier that protects intestinal tissue from invading intraluminal bacteria [8-10]. IEC
71 death disrupts intestinal homeostasis in some mouse models [11-18], and excessive IEC death
72 is observed in patients with IBDs [19, 20]. In addition, macrophages, major components of the
73 innate immune system that reside just beneath IECs, play crucial roles as the first line of defense
74 [21-24]. When intestinal homeostasis is perturbed by genetic or environmental factors such as
75 epithelial barrier disruption or macrophage dysregulation, a large number of TLR-expressing
76 pro-inflammatory macrophages migrate into the inflamed mucosa and release pro-
77 inflammatory cytokines and chemokines such as IL-6, [TNF](#), and MCP-1/CCL2 [22-24] in
78 response to products derived from invading bacteria [25]. Although appropriate responses
79 confer protection against bacteria and promote tissue regeneration by acting on other immune
80 cells and IECs, uncontrolled responses lead to persistent inflammation, which inhibits tissue
81 repair [22-24, 26-28].

82 The linear ubiquitin chain assembly complex (LUBAC), comprising HOIP, HOIL-1L, and
83 SHARPIN, activates the NF- κ B signaling pathway and inhibits [programmed cell death by](#)
84 [generating](#) unique N-terminal-linked linear polyubiquitin chains via the catalytic center in

85 HOIP [29-32]. Several reports suggest that NF- κ B activation maintains IEC homeostasis by
86 inhibiting IEC death; however, activation of NF- κ B in macrophages plays a pro-inflammatory
87 role [33-36]. Recent genome-wide association studies also show that NF- κ B is associated with
88 IBDs [37]. Despite the essential roles played by NF- κ B and cell death during intestinal
89 inflammation, involvement of LUBAC-mediated linear ubiquitination is unclear.

90 Considering the cell type-specific roles of both NF- κ B and cell death [33, 38], we used mice
91 lacking the C-terminal catalytic center of HOIP specifically in IECs (HOIP^{IEC- Δ lin}) or
92 macrophages (HOIP^{MYE- Δ lin}) to examine the role of linear ubiquitination in IECs and
93 macrophages. Since no spontaneous intestinal phenotype was observed in either mouse model,
94 we used mouse models of IBD generated by intraperitoneal administration of LPS or by oral
95 administration of dextran sodium sulphate (DSS) [39, 40]. Loss of ligase activity in IECs
96 provoked mucosal inflammation and augmented TNF-mediated IEC death upon LPS
97 administration, indicating that linear ubiquitination in IECs protects against intestinal
98 inflammation and suppresses TNF-induced IEC death under inflammatory conditions. By
99 contrast, loss of LUBAC ligase activity in macrophages alleviated DSS-induced colitis and
100 impaired NF- κ B- and ERK-mediated inflammatory cytokine production upon TLR stimulation,
101 indicating that linear ubiquitination in macrophages augments intestinal inflammation in the
102 event of an epithelial barrier breach. These findings demonstrate that linear ubiquitination in
103 IECs and macrophages plays differential roles to maintain both TNF-mediated epithelial
104 integrity and macrophage pro-inflammatory responses to regulate intestinal inflammation.

105 **Materials and methods**

106 Mice

107 HOIP^{Δlin-flox/Δlin-flox} mice, in which the C-terminal catalytic center of HOIP (*Rnf31*) is flanked
108 by two *loxP* sites, have been described previously [41, 42]. HOIP^{Δlin-flox/Δlin-flox} mice were
109 crossed with *Villin-Cre* [43] or *LysM-Cre* [44] mice to ablate the ligase activity of HOIP in IECs
110 or macrophages, respectively. Unless specified otherwise, mice (aged 8 to 12 weeks) were
111 cohoused with sex-matched littermates under specific pathogen-free conditions. All animal
112 protocols were approved by Kyoto University.

113

114 Antibodies

115 The antibodies used in this study are listed in Supplementary materials and methods.

116

117 LPS and TNF-induced IEC death

118 Mice were injected intraperitoneally with LPS (10 μg/g bodyweight (BW), *Escherichia coli*
119 055:B5; Sigma-Aldrich, St. Louis, MO, USA) or recombinant mouse TNF-α (0.1 μg/g BW;
120 R&D Systems, Minneapolis, MN, USA).

121

122 TNF depletion experiments

123 Mice were injected intraperitoneally with an anti-TNF-α antibody (200 μg, clone XT3.11; Bio
124 X Cell, Lebanon, NH, USA) or an isotype control IgG (200 μg, clone TNP6A7; Bio X Cell) 1
125 h before LPS challenge.

126

127 Induction of colitis

128 Experimental colitis was induced by oral administration of 2.0% or 1.5% DSS (MP Biomedicals,
129 Irvine, CA, USA) dissolved in drinking water (ingested for 7 or 5 days), followed by of normal

130 water (ingested for 2 or 5 days).

131

132 Histological analysis

133 The distal third of the colon or ileal segment was fixed in 10% formalin and embedded in
134 paraffin. The severity of DSS-induced colitis was determined by examining H&E-stained
135 sections, as described previously [45]. Multiple viewing fields per slide were acquired
136 randomly under an Olympus BX51 upright microscope (Olympus, Tokyo, Japan) or a
137 FLUOVIEW FV1000 confocal laser scanning microscope (Olympus).

138

139 IEC isolation and organoid culture

140 IEC isolation and generation of organoids were performed as previously described [46]. To
141 examine cell death, cells were stained with 5 μ M SYTOX Green nucleic acid stain (Invitrogen,
142 Waltham, MA, USA) and 5 μ g/ml Hoechst 33342 nucleic acid stain (Invitrogen), which were
143 added to the medium, followed by observation under an IX83 Inverted Research Microscope
144 (Olympus). Organoids were treated with LPS (Sigma-Aldrich) or TNF- α (R&D Systems). Z-
145 VAD-FMK (ZVAD) (PEPTIDE, Osaka, Japan) was added 1 h before TNF treatment.

146

147 Enrichment of bone marrow-derived macrophages

148 Bone marrow-derived macrophages (BMDMs) were isolated from bone marrow from the tibia
149 and femur and cultured for 7 days in complete RPMI containing 20 ng/ml recombinant murine
150 M-CSF (BioLegend, San Diego, CA, USA). BMDMs were stimulated with TNF, LPS,
151 Poly(I:C) (InvivoGen, San Diego, CA, USA), CpG-B (InvivoGen), or Pam3CSK4 (InvivoGen).
152 For some experiments, HOIPin-8 (Axon Medchem LLC, Reston, VA, USA) or a MEK inhibitor
153 (PD0325901; FUJIFILM, Osaka, Japan) was added before stimulation.

154

155 Statistical analysis

156 Results are expressed as the mean \pm SEM. Statistical analyses were performed using

157 GraphPad Prism Version9.3.1 (GraphPad Software, San Diego, CA, USA). All statistical tests

158 are indicated in each figure legend. The significance level was set at $P < 0.05$.

159

160 **Results**

161 **Mice lacking linear ubiquitination activity in IECs display mucosal inflammation and**
162 **augmented IEC death upon intraperitoneal administration of LPS**

163 To investigate the role of LUBAC-mediated linear ubiquitination in IECs, we crossed
164 HOIP^{Δlin-flox/Δlin-flox} mice [41, 42] with *Villin-Cre* mice [43] to delete the linear ubiquitination
165 activity of LUBAC (HOIP Δlinear) specifically in IECs (HOIP^{IEC-Δlin} mice) (supplementary
166 material, Figure S1A). Immunoblotting revealed that *Cre*-mediated recombination of HOIP loci
167 (*Rnf31*), as evaluated by the decrease in full-length HOIP, was not complete (expression of full-
168 length HOIP in the colon and the small intestine of HOIP^{IEC-Δlin} mice was 49.2 ± 2.1% and 28.8
169 ± 3.7%, respectively, of that observed in control HOIP^{Δlin-flox/Δlin-flox} mice; supplementary
170 material, Figure S1B). This was also the case for organoid cultures (31.5 ± 5.4% expression in
171 HOIP^{IEC-Δlin} organoids compared with control organoids; supplementary material, Figure S1B).
172 The amounts of HOIL-1L and SHARPIN, the other two subunits of LUBAC, were also reduced
173 (supplementary material, Figure S1B). HOIP^{IEC-Δlin} mice developed normally (supplementary
174 material, Figure S1C); however, whole-body deletion of HOIP was embryonic lethal [47, 48].
175 There were no overt changes in tissue architecture, nor defects in IEC differentiation, in the
176 colon or small intestine under steady-state conditions (supplementary material, Figure S1D–F).

177 Intraperitoneal administration of LPS causes shedding of IECs in the small intestine
178 [39, 49]. LUBAC-mediated linear ubiquitination plays a role in protecting cells from
179 programmed cell death [30, 32, 50, 51]. We found that HOIP^{IEC-Δlin} mice were extremely
180 sensitive to intraperitoneal administration of LPS; these mice showed a significant reduction in
181 colon length, and marked mucosal damage in the distal colon, at 24 h post-LPS treatment
182 (Figure 1A, B). Immunohistological analysis revealed increased infiltration of the distal colon
183 by leukocytes, including macrophages (Figure 1C, D and supplementary material, Figure S2).
184 Moreover, at 4 h post-LPS administration the number of apoptotic cells that were cleaved

185 caspase 3- and TUNEL-positive was higher in the distal colon of HOIP^{IEC-Δlin} mice than in that
186 of control mice, although there was no difference in the number of apoptotic cells under steady-
187 state conditions (Figure 1E, F). In particular, apoptotic cells were detected in all layers of the
188 distal colon, including the crypt bottom, in HOIP^{IEC-Δlin} mice (Figure 1E, F). The inflammatory
189 changes in the distal colon in HOIP^{IEC-Δlin} mice were not observed in the small intestine
190 (supplementary material, Figure S3A). However, apoptotic cells were detected in the crypts and
191 villous tips in HOIP^{IEC-Δlin} small intestine at 1.5 h post-LPS administration, along with an
192 increase in the number of apoptotic IECs; however, apoptotic cells were observed only at the
193 villous tips in the small intestine of control mice, regardless of LPS administration
194 (supplementary material, Figure S3B, C) [39, 52]. Taken together, these data suggest that loss
195 of LUBAC ligase activity in IECs renders mice more sensitive to IEC death in the colon and
196 small intestine after intraperitoneal injection of LPS, which may lead to mucosal inflammation
197 (although no inflammatory changes were observed in the small intestine).

198

199 **TNF drives LPS-induced mucosal inflammation and augmented IEC death in mice** 200 **lacking epithelial LUBAC ligase activity**

201 To examine the mechanism underlying IEC death in LPS-treated HOIP^{IEC-Δlin} mice,
202 we established intestinal epithelial organoids. There were no morphological differences
203 between HOIP^{IEC-Δlin} and control organoids, and LPS-treatments induced no apparent
204 morphological changes in the organoids (Figure 2A). Because shedding of IECs is thought to
205 be triggered by inflammatory cytokines produced by LPS-stimulated macrophages [39, 49],
206 and LUBAC-mediated linear ubiquitination protects cells from TNF-induced cell death
207 (including apoptosis and necroptosis) [30, 32, 50, 51], we focused on TNF as LPS
208 administration induced expression of TNF in the serum and colon tissues of HOIP^{IEC-Δlin} and
209 control mice (Figure 2B, C). We found that HOIP^{IEC-Δlin} organoids exhibited a disrupted and

210 dark appearance as early as 24 h after TNF treatment (Figure 2A). After treatment with TNF,
211 the proportion of SYTOX Green-positive organoids was higher for HOIP^{IEC-Δlin} than for
212 controls, indicating that TNF, but not LPS, is responsible for cell death in HOIP^{IEC-Δlin} organoids
213 (Figure 2A). Immunoblotting revealed that cleavage of both caspase 8 and 3 was higher in TNF-
214 treated HOIP^{IEC-Δlin} organoids, whereas phosphorylation of MLKL, an executor of necroptosis,
215 was not detected in either HOIP^{IEC-Δlin} or control organoids (Figure 2D). These data suggest that
216 TNF preferentially triggers apoptosis of HOIP^{IEC-Δlin} organoids. In addition, degradation of
217 IκBα, a hallmark of NF-κB activation, was impaired substantially in HOIP^{IEC-Δlin} organoids
218 upon TNF stimulation (Figure 2E), and expression of NF-κB target genes, including anti-
219 apoptotic genes, was partially attenuated in HOIP^{IEC-Δlin} organoids exposed to TNF (Figure 2F).
220 These results indicate that loss of LUBAC ligase activity sensitizes organoids to TNF-induced
221 apoptosis (at least in part) by impairing NF-κB activation.

222 Intraperitoneal injections of TNF provoked mucosal inflammation in the colon of
223 HOIP^{IEC-Δlin} mice, with shortening of the colon and increased invasion by inflammatory cells;
224 this was not observed in control mice (Figure 3A–D and supplementary material, Figure S2).
225 Immunohistochemical analysis revealed increased numbers of cleaved caspase 3-positive IECs
226 in the colon of HOIP^{IEC-Δlin} mice (Figure 3E). Although H&E staining revealed that changes in
227 the small intestine of HOIP^{IEC-Δlin} mice were less pronounced than those in the colon
228 (supplementary material, Figure S3D), cleaved caspase 3-positive apoptotic cells in the small
229 intestine of TNF-treated HOIP^{IEC-Δlin} mice were observed at the crypt bottom and the villous
230 tips (supplementary material, Figure S3E, F). Pretreatment with the anti-TNF antibody
231 prevented LPS-induced inflammatory changes in HOIP^{IEC-Δlin} mice, including shortening of the
232 colon, infiltration of the colon by immune cells and apoptosis of IECs (Figure 3F–J and
233 supplementary material, Figure S3G–I). Collectively, these results indicate that LUBAC-

234 induced linear ubiquitination protects mice from LPS-induced mucosal inflammation and TNF-
235 induced IEC death.

236

237 **Defective LUBAC catalytic activity in macrophages, but not in IECs, ameliorates DSS-**
238 **induced colitis**

239 To examine whether IEC death in HOIP^{IEC-Δlin} mice has an effect on the phenotype
240 of another mouse model of IBD, we fed HOIP^{IEC-Δlin} and control mice with 2% or 1.5% DSS, a
241 direct chemical toxin to IECs [53], for 7 or 5 days. However, loss of the LUBAC ligase activity
242 in IECs did not overtly affect severity of DSS-induced colitis (including BW changes,
243 shortening of the colon, histological changes, or expression of inflammatory cytokines) (Figure
244 4A–D and supplementary material, Figure S4). In addition, we examined apoptotic IECs in
245 DSS-treated HOIP^{IEC-Δlin} mice, and observed cleaved caspase 3- and TUNEL-positive IECs in
246 some crypts that escaped DSS-induced direct injury (Figure 4E). Thus, we suspect that loss of
247 linear ubiquitination activity in IECs does not overtly affect the severity of DSS-induced colitis,
248 despite the tendency toward increased IEC death; this may be because DSS damages IECs
249 directly.

250 Next, we examined the role played by linear ubiquitination in macrophages during
251 intestinal inflammation because macrophages represent the first line of defense after epithelial
252 barrier disruption [24]. To this end, we crossed HOIP^{Δlin-flox/Δlin-flox} mice with *LysM-Cre* mice
253 [44] to generate mice lacking the catalytic center of HOIP specifically in macrophages
254 (HOIP^{MYE-Δlin}). We observed a marked reduction ($44.2 \pm 0.7\%$) in expression of full-length
255 HOIP, along with HOIL-1L and SHARPIN, in HOIP^{MYE-Δlin} BMDMs compared with control
256 BMDMs (supplementary material, Figure S5A, B). This was also the case for peritoneal
257 macrophages, in which expression of full-length HOIP in HOIP^{MYE-Δlin} mice was attenuated
258 significantly, albeit not completely (supplementary material, Figure S5A). HOIP^{MYE-Δlin} mice

259 developed normally, and no inflammatory or autoimmune phenotypes were observed in the
260 intestine or the skin of aged HOIP^{MYE-Δlin} mice (supplementary material, Figure S5C, D).
261 Additionally, there was no abnormality in the proportions of activated lymphocytes, including
262 germinal center B cells (PNA⁺FAS⁺), activated T cells (CD25⁺CD69⁺), or effector T cells
263 (CD44^{hi}CD62L^{lo}), in the spleen or peripheral lymph nodes of aged HOIP^{MYE-Δlin} mice
264 (supplementary material, Figure S6).

265 To evaluate involvement of linear ubiquitination in macrophages after an epithelial
266 barrier breach, we fed HOIP^{MYE-Δlin} and control mice with DSS. We found that inflammatory
267 changes, including weight loss and shortening of the colon, were less severe in HOIP^{MYE-Δlin}
268 mice than in control mice (Figure 5A, B). Histological analysis revealed that mucosal damage
269 in the distal colon was less severe in HOIP^{MYE-Δlin} mice than in control mice (Figure 5C).
270 Immunohistological analysis also showed that the number of the leukocytes, including
271 macrophages, B cells, and T cells, was lower in DSS-treated HOIP^{MYE-Δlin} mice (Figure 5D, E
272 and supplementary material, Figure S7). Moreover, expression of inflammatory cytokines in
273 the colon was significantly lower (Figure 5F). Next, we injected HOIP^{MYE-Δlin} and control mice
274 intraperitoneally with LPS, because macrophages are thought to be involved in the pathogenesis
275 of the LPS-induced IEC shedding [39]. However, regardless of LUBAC ligase activity, we
276 found no overt differences in the number of apoptotic IECs in the small intestine, or the levels
277 of inflammatory cytokines in serum or intestinal tissue (supplementary material, Figure S8).
278 Collectively, the data suggest that attenuated linear ubiquitination in macrophages ameliorates
279 the severity of colitis after an epithelial breach induced by DSS.

280

281 **Attenuation of LUBAC ligase activity in macrophages impairs NF-κB- and ERK-**
282 **mediated production of inflammatory cytokines in response to TLR stimulation**

283 To address the molecular mechanisms underlying amelioration of DSS-induced
284 colitis in HOIP^{MYE-Δlin} mice, we stimulated BMDMs from HOIP^{MYE-Δlin} and control mice with
285 TNF [30-32]. We found that phosphorylation and degradation of IκBα, as well as
286 phosphorylation of p65 and IKK, were lower in TNF-stimulated HOIP^{MYE-Δlin} BMDMs than in
287 control BMDMs (Figure 6A). Studies suggest that TLRs expressed by pro-inflammatory
288 macrophages play a role in DSS-induced colitis [22, 23]. Upon LPS stimulation, not only
289 phosphorylation and degradation of IκBα, but also phosphorylation of IKK and p65, was
290 impaired in HOIP^{MYE-Δlin} BMDMs (Figure 6B), indicating that loss of LUBAC ligase activity
291 in macrophages attenuates LPS-mediated activation of NF-κB. IKK activation in macrophages
292 leads to activation of ERK [42, 54, 55]; here, we found that LPS-induced phosphorylation of
293 ERK was lower in HOIP^{MYE-Δlin} BMDMs than in control BMDMs (Figure 6C). By contrast,
294 loss of LUBAC ligase activity did not overtly affect activation of other MAPK pathways,
295 including p38 and JNK (Figure 6C). To confirm the role of LUBAC-mediated linear
296 ubiquitination during LPS signaling in macrophages, we treated BMDMs from WT mice with
297 HOIPin-8, a specific inhibitor of LUBAC ligase activity [56]. As shown in Figure 6D, LPS-
298 mediated activation of NF-κB and ERK was attenuated markedly by HOIPin-8, whereas
299 activation of JNK and p38 was not. These results indicate that linear ubiquitination is involved
300 in LPS-triggered activation of NF-κB and ERK, but not p38 or JNK, in macrophages.
301 Augmented cell death is observed in some cells with attenuated LUBAC activity [30, 32, 50,
302 51]. However, linear ubiquitination in macrophages has no obvious effect on TNF-mediated
303 cell death, regardless of the presence of cycloheximide, or LPS-induced cell death in HOIP<sup>MYE-
304 Δlin</sup> BMDMs, or DSS-treated HOIP^{MYE-Δlin} mice (supplementary material, Figure S9).

305 Next, we asked how loss of linear ubiquitination affects inflammatory cytokine
306 production upon TLR stimulation. LPS-induced production of IL-6, TNF, and MCP-1/CCL2
307 (a chemoattractant for macrophages) fell significantly in HOIP^{MYE-Δlin} BMDMs and HOIPin-8-

308 treated BMDMs from WT mice (Figure 6E, F). Because treatment with a MEK inhibitor
309 suppressed TNF and MCP-1/CCL2 (Figure 6G), we speculated that ERK acts synergistically
310 with NF- κ B to trigger production of inflammatory cytokines. Lastly, we investigated LUBAC
311 involvement in other TLR signaling pathways. Upon stimulation with TLR ligands Poly(I:C),
312 CpG-B, or Pam3CSK4, phosphorylation and degradation of I κ B α , and phosphorylation of IKK
313 and p65, was substantially attenuated by pretreatment with HOIPin-8 (supplementary material,
314 Figure S10). ERK activation was impaired markedly by HOIPin-8 downstream of these ligands
315 (supplementary material, Figure S10). Furthermore, production of IL-6 by HOIP^{MYE- Δ lin}
316 BMDMs was impaired substantially in response to Poly(I:C), CpG-B, and Pam3CSK4 (Figure
317 6H), suggesting that linear ubiquitination is involved in signaling via multiple TLRs.
318 Collectively, these results suggest that linear ubiquitination in macrophages augments intestinal
319 inflammation in the event of an epithelial barrier breach induced by DSS, possibly due to
320 increased production of pro-inflammatory cytokines and a macrophage chemoattractant
321 downstream of NF- κ B and ERK pathway activation by multiple TLR ligands.

322 Discussion

323 Dysfunction of the epithelial barrier and unrestrained inflammatory responses by macrophages
324 are major factors contributing to the pathogenesis of IBDs [22-24, 57]. Since cell-specific
325 targeting is vital to uncover the roles of NF- κ B- and cell death-related pathways [33, 38], we
326 examined the role of LUBAC ligase activity, which controls NF- κ B activation and programmed
327 cell death [29-32], in both IECs and macrophages during intestinal inflammation. To do this,
328 we used two experimental mouse models of IBD. Loss of the LUBAC ligase activity in IECs
329 or macrophages resulted in different phenotypes: IEC-specific loss of linear ubiquitination
330 activity sensitized mice to mucosal inflammation after LPS administration, whereas loss of
331 activity in macrophages ameliorated DSS-induced colitis.

332 Mice with IEC-specific deletion of molecules essential for NF- κ B activation or protection
333 from TNF-mediated cell death exhibit spontaneous severe intestinal inflammation due to the
334 augmented sensitivity to TNF-induced cell death [11, 14]. However, HOIP^{IEC- Δ lin} mice did not
335 develop spontaneous histological abnormalities in the intestines (supplementary material,
336 Figure S1D–F), despite the crucial role of LUBAC-mediated linear ubiquitination in NF- κ B
337 activation and protection from cell death [32, 50, 51]. Observations in the intestines of HOIP^{IEC-}
338 ^{Δ lin} mice were in sharp contrast to those in skin (another border between the environment and
339 the body), in which attenuated LUBAC function triggers spontaneous dermatitis due to TNF-
340 mediated cell death [50, 58, 59]. The mechanisms responsible for the discrepancy between the
341 skin and intestine are unknown; however, the finding that LUBAC ligase activity in IECs is
342 dispensable for intestinal homeostasis enabled us to evaluate two IBD models: LPS-mediated
343 IEC shedding and DSS-induced colitis [39, 40]. Loss of the LUBAC ligase activity in IECs
344 rendered mice susceptible to mucosal inflammation and augmented IEC death upon
345 intraperitoneal injection of LPS (Figure 1); this was phenocopied by TNF injection (Figure 3A–
346 E), and was rescued by an anti-TNF antibody (Figure 3F–J). We also found that TNF induced

347 apoptosis of HOIP^{IEC-Δlin} organoids; however, LPS did not (Figure 2A, D), which was due in
348 part to the compromised NF-κB pathway (Figure 2E, F). At present, we do not know why we
349 could not detect inflammation in the small intestine of LPS-treated HOIP^{IEC-Δlin} mice, despite
350 augmented epithelial apoptosis (supplementary material, Figure S3A–C). However,
351 mechanisms other than NF-κB- or LUBAC-mediated pathways may act to maintain integrity
352 of the small intestine. TNF is involved in the pathogenesis of IBDs in humans because TNF-
353 targeted therapy is a highly effective treatment [60], and TNF is also a potent driver of epithelial
354 barrier disruption [11, 14, 17, 20, 61]. Our results clearly highlight a crucial role for LUBAC-
355 mediated linear ubiquitination in maintaining TNF-induced epithelial integrity under
356 inflammatory conditions (supplementary material, Figure S11).

357 In contrast to the LPS-induced IEC shedding model, HOIP^{IEC-Δlin} mice did not exhibit obvious
358 sensitivity to DSS-induced colitis (Figure 4A–D). In this model, mice receive oral DSS for
359 several days; however, in the LPS-induced IEC shedding model, IEC shedding is usually
360 evaluated within 1 day of LPS administration [15, 39, 40, 49]. We found that HOIP^{IEC-Δlin} mice
361 displayed mucosal inflammation within 24 h of LPS administration (Figure 1). Moreover, it is
362 suspected that administration of DSS, a direct chemical toxin to IECs, for several days leads to
363 massive disruption of IECs [53], which might suggest that augmented sensitivity to intestinal
364 inflammation and IEC death in HOIP^{IEC-Δlin} mice cannot be properly evaluated by DSS
365 administration. Therefore, the DSS-induced colitis model alone may not be suitable for probing
366 the mechanism underlying disruption of epithelial integrity within a short time. An LPS-
367 induced IEC shedding model together with DSS-induced colitis model might be more beneficial
368 for evaluating the pathogenesis of IBDs.

369 Pro-inflammatory macrophages accumulate and respond in a highly pro-inflammatory manner
370 to stimulation of TLR ligands after epithelial disruption induced by DSS [22, 23]. In contrast
371 to HOIP^{IEC-Δlin} mice (Figure 4), HOIP^{MYE-Δlin} mice displayed attenuated mucosal damage and

372 less infiltration by immune cells, as well as induction of inflammatory cytokines, upon DSS-
373 induced epithelial injury (Figure 5). We observed that loss of the LUBAC ligase activity in
374 BMDMs stimulated with LPS led to decreased production of macrophage chemoattractant
375 MCP-1/CCL2, as well as pro-inflammatory IL-6 and TNF, downstream of attenuated NF-κB
376 and ERK activation (Figure 6). Since loss of the LUBAC ligase activity did not overtly augment
377 macrophage death (supplementary material, Figure S9), downregulated expression of MCP-
378 1/CCL2 (Figure 5F and 6E, F), not induction of cell death, is likely responsible for decreased
379 accumulation of macrophages (Figure 5D, E), which might further attenuate inflammatory
380 responses in DSS-treated HOIP^{MYE-Δlin} mice. Collectively, the data suggest that linear
381 ubiquitination in macrophages augments intestinal inflammation in the event of an epithelial
382 barrier breach by promoting recruitment of macrophages to sites of damage, as well as by up-
383 regulating production of pro-inflammatory cytokines via activation of the NF-κB and ERK
384 pathways (supplementary material, Figure S11).

385 **By contrast, IEC shedding** upon intraperitoneal injection of LPS was comparable in HOIP^{MYE-}
386 ^{Δlin} and control mice (supplementary material, Figure S8A). This might be because there is no
387 overt difference in expression of inflammatory cytokines between LPS-treated HOIP^{MYE-Δlin}
388 and control mice (supplementary material, Figure S8B, C). We suspected that dendritic cells,
389 effector T cells, adipocytes, and fibroblasts (in addition to macrophages) might produce IL-6
390 and TNF upon LPS injection because these cells produce these cytokines as a direct or indirect
391 response to LPS [26, 27]. Macrophages play pleiotropic roles during acute inflammation,
392 including activation of other immune cells, elimination of infectious agents, and promotion of
393 tissue regeneration, whereas prolonged inflammation delays tissue repair [22-24, 26-28]. Thus,
394 loss of LUBAC ligase activity in macrophages may prevent prolonged inflammation and
395 facilitate epithelial repair in DSS-induced colitis (Figure 5) without affecting acute
396 inflammatory responses that are necessary for tissue regeneration.

397 In conclusion, we show here that linear ubiquitination in IECs and macrophages plays a role
398 in the pathogenesis of IBDs. While direct epithelial injury by DSS administration is useful for
399 investigate macrophage function as the first line of defense in the innate immune system, rapid
400 and indirect IEC shedding induced by LPS administration might also be a suitable option for
401 investigating the mechanisms that maintain epithelial integrity. Linear ubiquitination in IECs
402 and macrophages functions differentially during intestinal inflammation by regulating TNF-
403 mediated epithelial integrity and macrophage pro-inflammatory responses, respectively;
404 therefore, cell-specific targeting of linear ubiquitination might be a novel approach to treating
405 IBDs.

406 **Acknowledgments**

407 We thank the Center for Anatomical, Pathological and Forensic Medical Research, Kyoto
408 University Graduate School of Medicine, for preparing tissue sections. We also thank Drs. S.
409 Kuno, Y. Shinkawa, Y. Fuseya, T. Jo, Y. Takeda, I. Yanatori, H. Fujita, and M. Kim for insightful
410 discussion and advice, and Ms Y. Akasaki, Y. Hayamizu, and N. Ueno for technical assistance.
411 This work was supported by JSPS KAKENHI Grant Numbers 17H06174 and 18H05499 (to K.
412 I.).

413

414 **Author contributions**

415 Y. S., Y. N., K. S., and K. I. conceived and designed the study. Y. S. performed the experiments.
416 M. O. and K. H. supported organoid culture. Y. I., K. K., K. O., and H. S. provided crucial
417 advice. Y. S. and K. I. wrote the manuscript, with contributions from all other authors.

418

419 **References**

- 420 1. Collaborators GBDIBD. The global, regional, and national burden of inflammatory
421 bowel disease in 195 countries and territories, 1990-2017: a systematic analysis for the Global
422 Burden of Disease Study 2017. *Lancet Gastroenterol Hepatol* 2020; **5**: 17-30.
- 423 2. Sartor RB. Mechanisms of disease: pathogenesis of Crohn's disease and ulcerative
424 colitis. *Nat Clin Pract Gastroenterol Hepatol* 2006; **3**: 390-407.
- 425 3. de Souza HS, Fiocchi C. Immunopathogenesis of IBD: current state of the art. *Nat*
426 *Rev Gastroenterol Hepatol* 2016; **13**: 13-27.
- 427 4. Chang JT. Pathophysiology of Inflammatory Bowel Diseases. *N Engl J Med* 2020;
428 **383**: 2652-2664.
- 429 5. Geremia A, Biancheri P, Allan P, *et al*. Innate and adaptive immunity in
430 inflammatory bowel disease. *Autoimmun Rev* 2014; **13**: 3-10.
- 431 6. Schey R, Danzer C, Mattner J. Perturbations of mucosal homeostasis through
432 interactions of intestinal microbes with myeloid cells. *Immunobiology* 2015; **220**: 227-235.
- 433 7. Baillie JK, Arner E, Daub C, *et al*. Analysis of the human monocyte-derived
434 macrophage transcriptome and response to lipopolysaccharide provides new insights into
435 genetic aetiology of inflammatory bowel disease. *PLoS Genet* 2017; **13**: e1006641.
- 436 8. Artis D. Epithelial-cell recognition of commensal bacteria and maintenance of
437 immune homeostasis in the gut. *Nat Rev Immunol* 2008; **8**: 411-420.
- 438 9. Turner JR. Intestinal mucosal barrier function in health and disease. *Nat Rev*
439 *Immunol* 2009; **9**: 799-809.
- 440 10. Peterson LW, Artis D. Intestinal epithelial cells: regulators of barrier function and
441 immune homeostasis. *Nat Rev Immunol* 2014; **14**: 141-153.
- 442 11. Nenci A, Becker C, Wullaert A, *et al*. Epithelial NEMO links innate immunity to
443 chronic intestinal inflammation. *Nature* 2007; **446**: 557-561.

- 444 12. Welz PS, Wullaert A, Vlantis K, *et al.* FADD prevents RIP3-mediated epithelial cell
445 necrosis and chronic intestinal inflammation. *Nature* 2011; **477**: 330-334.
- 446 13. Dannappel M, Vlantis K, Kumari S, *et al.* RIPK1 maintains epithelial homeostasis
447 by inhibiting apoptosis and necroptosis. *Nature* 2014; **513**: 90-94.
- 448 14. Takahashi N, Vereecke L, Bertrand MJ, *et al.* RIPK1 ensures intestinal homeostasis
449 by protecting the epithelium against apoptosis. *Nature* 2014; **513**: 95-99.
- 450 15. Gunther C, Buchen B, He GW, *et al.* Caspase-8 controls the gut response to
451 microbial challenges by Tnf- α -dependent and independent pathways. *Gut* 2015; **64**: 601-610.
- 452 16. Eftychi C, Schwarzer R, Vlantis K, *et al.* Temporally Distinct Functions of the
453 Cytokines IL-12 and IL-23 Drive Chronic Colon Inflammation in Response to Intestinal
454 Barrier Impairment. *Immunity* 2019; **51**: 367-380 e364.
- 455 17. Schwarzer R, Jiao H, Wachsmuth L, *et al.* FADD and Caspase-8 Regulate Gut
456 Homeostasis and Inflammation by Controlling MLKL- and GSDMD-Mediated Death of
457 Intestinal Epithelial Cells. *Immunity* 2020; **52**: 978-993 e976.
- 458 18. Nakanishi Y, Reina-Campos M, Nakanishi N, *et al.* Control of Paneth Cell Fate,
459 Intestinal Inflammation, and Tumorigenesis by PKC λ / ι . *Cell Rep* 2016; **16**: 3297-3310.
- 460 19. Iwamoto M, Koji T, Makiyama K, *et al.* Apoptosis of crypt epithelial cells in
461 ulcerative colitis. *J Pathol* 1996; **180**: 152-159.
- 462 20. Gunther C, Martini E, Wittkopf N, *et al.* Caspase-8 regulates TNF- α -induced
463 epithelial necroptosis and terminal ileitis. *Nature* 2011; **477**: 335-339.
- 464 21. Smith PD, Smythies LE, Shen R, *et al.* Intestinal macrophages and response to
465 microbial encroachment. *Mucosal Immunol* 2011; **4**: 31-42.
- 466 22. Bain CC, Mowat AM. Macrophages in intestinal homeostasis and inflammation.
467 *Immunol Rev* 2014; **260**: 102-117.
- 468 23. Bain CC, Schridde A. Origin, Differentiation, and Function of Intestinal

- 469 Macrophages. *Front Immunol* 2018; **9**: 2733.
- 470 24. Na YR, Stakenborg M, Seok SH, *et al.* Macrophages in intestinal inflammation and
471 resolution: a potential therapeutic target in IBD. *Nat Rev Gastroenterol Hepatol* 2019; **16**:
472 531-543.
- 473 25. Akira S, Uematsu S, Takeuchi O. Pathogen recognition and innate immunity. *Cell*
474 2006; **124**: 783-801.
- 475 26. Friedrich M, Pohin M, Powrie F. Cytokine Networks in the Pathophysiology of
476 Inflammatory Bowel Disease. *Immunity* 2019; **50**: 992-1006.
- 477 27. Neurath MF. Cytokines in inflammatory bowel disease. *Nat Rev Immunol* 2014; **14**:
478 329-342.
- 479 28. Karin M, Clevers H. Reparative inflammation takes charge of tissue regeneration.
480 *Nature* 2016; **529**: 307-315.
- 481 29. Kirisako T, Kamei K, Murata S, *et al.* A ubiquitin ligase complex assembles linear
482 polyubiquitin chains. *EMBO J* 2006; **25**: 4877-4887.
- 483 30. Tokunaga F, Sakata S, Saeki Y, *et al.* Involvement of linear polyubiquitylation of
484 NEMO in NF- κ B activation. *Nat Cell Biol* 2009; **11**: 123-132.
- 485 31. Iwai K, Tokunaga F. Linear polyubiquitination: a new regulator of NF- κ B
486 activation. *EMBO Rep* 2009; **10**: 706-713.
- 487 32. Ikeda F, Deribe YL, Skanland SS, *et al.* SHARPIN forms a linear ubiquitin ligase
488 complex regulating NF- κ B activity and apoptosis. *Nature* 2011; **471**: 637-641.
- 489 33. Greten FR, Eckmann L, Greten TF, *et al.* IKK β links inflammation and
490 tumorigenesis in a mouse model of colitis-associated cancer. *Cell* 2004; **118**: 285-296.
- 491 34. Atreya I, Atreya R, Neurath MF. NF- κ B in inflammatory bowel disease. *J Intern*
492 *Med* 2008; **263**: 591-596.
- 493 35. Pasparakis M. Regulation of tissue homeostasis by NF- κ B signalling: implications

494 for inflammatory diseases. *Nat Rev Immunol* 2009; **9**: 778-788.

495 36. Liu T, Zhang L, Joo D, *et al.* NF- κ B signaling in inflammation. *Signal Transduct*
496 *Target Ther* 2017; **2**.

497 37. Jostins L, Ripke S, Weersma RK, *et al.* Host-microbe interactions have shaped the
498 genetic architecture of inflammatory bowel disease. *Nature* 2012; **491**: 119-124.

499 38. Vereecke L, Vieira-Silva S, Billiet T, *et al.* A20 controls intestinal homeostasis
500 through cell-specific activities. *Nat Commun* 2014; **5**: 5103.

501 39. Williams JM, Duckworth CA, Watson AJ, *et al.* A mouse model of pathological
502 small intestinal epithelial cell apoptosis and shedding induced by systemic administration of
503 lipopolysaccharide. *Dis Model Mech* 2013; **6**: 1388-1399.

504 40. Chassaing B, Aitken JD, Malleshappa M, *et al.* Dextran sulfate sodium (DSS)-
505 induced colitis in mice. *Curr Protoc Immunol* 2014; **104**: 15 25 11-15 25 14.

506 41. Sasaki Y, Iwai K. Crucial Role of Linear Ubiquitin Chain Assembly Complex-
507 Mediated Inhibition of Programmed Cell Death in TLR4-Mediated B Cell Responses and B1b
508 Cell Development. *J Immunol* 2018; **200**: 3438-3449.

509 42. Sasaki Y, Sano S, Nakahara M, *et al.* Defective immune responses in mice lacking
510 LUBAC-mediated linear ubiquitination in B cells. *EMBO J* 2013; **32**: 2463-2476.

511 43. el Marjou F, Janssen KP, Chang BH, *et al.* Tissue-specific and inducible Cre-
512 mediated recombination in the gut epithelium. *Genesis* 2004; **39**: 186-193.

513 44. Clausen BE, Burkhardt C, Reith W, *et al.* Conditional gene targeting in
514 macrophages and granulocytes using LysMcre mice. *Transgenic Res* 1999; **8**: 265-277.

515 45. Nakatsuji M, Minami M, Seno H, *et al.* EP4 Receptor-Associated Protein in
516 Macrophages Ameliorates Colitis and Colitis-Associated Tumorigenesis. *PLoS Genet* 2015;
517 **11**: e1005542.

518 46. Sato T, Vries RG, Snippert HJ, *et al.* Single Lgr5 stem cells build crypt-villus

519 structures in vitro without a mesenchymal niche. *Nature* 2009; **459**: 262-265.

520 47. Peltzer N, Rieser E, Taraborrelli L, *et al.* HOIP deficiency causes embryonic
521 lethality by aberrant TNFR1-mediated endothelial cell death. *Cell Rep* 2014; **9**: 153-165.

522 48. Peltzer N, Darding M, Montinaro A, *et al.* LUBAC is essential for embryogenesis
523 by preventing cell death and enabling haematopoiesis. *Nature* 2018; **557**: 112-117.

524 49. Jones LG, Vaida A, Thompson LM, *et al.* NF- κ B2 signalling in enteroids modulates
525 enterocyte responses to secreted factors from bone marrow-derived dendritic cells. *Cell Death*
526 *Dis* 2019; **10**: 896.

527 50. Taraborrelli L, Peltzer N, Montinaro A, *et al.* LUBAC prevents lethal dermatitis by
528 inhibiting cell death induced by TNF, TRAIL and CD95L. *Nat Commun* 2018; **9**: 3910.

529 51. Tang Y, Joo D, Liu G, *et al.* Linear ubiquitination of cFLIP induced by LUBAC
530 contributes to TNF α -induced apoptosis. *J Biol Chem* 2018; **293**: 20062-20072.

531 52. Watson AJ, Hughes KR. TNF- α -induced intestinal epithelial cell shedding:
532 implications for intestinal barrier function. *Ann N Y Acad Sci* 2012; **1258**: 1-8.

533 53. Eichele DD, Kharbanda KK. Dextran sodium sulfate colitis murine model: An
534 indispensable tool for advancing our understanding of inflammatory bowel diseases
535 pathogenesis. *World J Gastroenterol* 2017; **23**: 6016-6029.

536 54. Gantke T, Sriskantharajah S, Sadowski M, *et al.* I κ B kinase regulation of the TPL-
537 2/ERK MAPK pathway. *Immunol Rev* 2012; **246**: 168-182.

538 55. Webb LV, Ventura S, Ley SC. ABIN-2, of the TPL-2 Signaling Complex, Modulates
539 Mammalian Inflammation. *Trends Immunol* 2019; **40**: 799-808.

540 56. Oikawa D, Sato Y, Ohtake F, *et al.* Molecular bases for HOIPINs-mediated
541 inhibition of LUBAC and innate immune responses. *Commun Biol* 2020; **3**: 163.

542 57. Vereecke L, Beyaert R, van Loo G. Enterocyte death and intestinal barrier
543 maintenance in homeostasis and disease. *Trends Mol Med* 2011; **17**: 584-593.

- 544 58. Kumari S, Redouane Y, Lopez-Mosqueda J, *et al.* Sharpin prevents skin
545 inflammation by inhibiting TNFR1-induced keratinocyte apoptosis. *Elife* 2014; **3**.
- 546 59. Rickard JA, Anderton H, Etemadi N, *et al.* TNFR1-dependent cell death drives
547 inflammation in Sharpin-deficient mice. *Elife* 2014; **3**.
- 548 60. Neurath MF. Current and emerging therapeutic targets for IBD. *Nat Rev*
549 *Gastroenterol Hepatol* 2017; **14**: 269-278.
- 550 61. Pott J, Kabat AM, Maloy KJ. Intestinal Epithelial Cell Autophagy Is Required to
551 Protect against TNF-Induced Apoptosis during Chronic Colitis in Mice. *Cell Host Microbe*
552 2018; **23**: 191-202 e194.
- 553
- 554

555 **Figure legends**

556 **Figure 1. Deletion of epithelial linear ubiquitination activity sensitizes mice to mucosal**
557 **inflammation and IEC death upon intraperitoneal administration of LPS.**

558 (A) Representative pictures (left) and quantification of colon length (right) in control and
559 HOIP^{IEC-Δlin} mice at the indicated times post-LPS treatment (n=3–5). ns, not significant.

560 (B) H&E staining of distal colon sections from control and HOIP^{IEC-Δlin} mice 24 h post-LPS
561 administration (n=3). Scale bars, 50 μm.

562 (C) Immunohistochemical staining for CD45 and F4/80 in the distal colon 4 h post-LPS
563 injection (n=3). Data from untreated control (UT) and HOIP^{IEC-Δlin} mice are also shown (n=3).

564 Yellow arrow heads depict cells positive for each marker. Scale bars, 50 μm.

565 (D) Quantification of immune cells in (C) (n=12 fields per group). Data from untreated control
566 and HOIP^{IEC-Δlin} mice are also shown (n=12 fields per group).

567 (E) Immunohistochemical staining for cleaved caspase 3 (Cl. Caspase3) in distal colon sections
568 4 h post-LPS treatment (n=3). Data from untreated control and HOIP^{IEC-Δlin} mice are also shown
569 (n=3). Scale bars, 50 μm.

570 (F) Immunofluorescence staining for TUNEL (green), E-cadherin (red), and DAPI (blue) in
571 distal colon sections 4 h post-LPS treatment (n=3). Data from untreated control and HOIP^{IEC-}
572 ^{Δlin} mice are also shown (n=3). Scale bars, 50 μm.

573 Statistical significance was determined by two-way ANOVA with Bonferroni's post-hoc test
574 (A, D). *P < 0.05, **P < 0.01, ***P < 0.005, ****P < 0.001.

575

576 **Figure 2. Intestinal epithelial organoids lacking LUBAC catalytic activity show evidence**
577 **of apoptosis upon treatment with TNF.**

578 (A) Representative images (top) obtained under a bright field microscope, SYTOX Green
579 staining, and Hoechst 33342 staining of organoids from control and HOIP^{IEC-Δlin} IECs treated

580 with PBS, LPS (100 ng/ml), or TNF (25 ng/ml) for 24 h. Percentage (bottom) of SYTOX Green-
581 positive organoids among total organoids. Data were obtained from a total of 30–50 organoids
582 per group. Experiments were performed at least three times independently. Scale bars, 100 μ m.
583 (B) ELISA to detect serum TNF levels in control and HOIP^{IEC- Δ lin} mice after intraperitoneal
584 injection of LPS (n=3).
585 (C) qRT-PCR analysis of *Tnf* mRNA levels in colon tissue from control and HOIP^{IEC- Δ lin} mice
586 after LPS administration (n=6). Data are normalized to expression of *Gapdh* mRNA.
587 (D) Organoids derived from control and HOIP^{IEC- Δ lin} mice were stimulated with TNF (40 ng/ml),
588 or pre-treated with ZVAD (20 μ M) for 1 h followed by treatment with TNF (40 ng/ml) for the
589 indicated times. Cell lysates were immunoblotted with the indicated antibodies. Tubulin was
590 used as a loading control.
591 (E) Organoids from control and HOIP^{IEC- Δ lin} mice were stimulated with TNF (40 ng/ml) for the
592 indicated times. Cell lysates were immunoblotted with the indicated antibodies. Tubulin was
593 used as a loading control.
594 (F) Organoids from control and HOIP^{IEC- Δ lin} IECs were stimulated with TNF (25 ng/ml) for the
595 indicated times, followed by qRT-PCR analysis of NF- κ B target gene mRNA (n=3). Data are
596 normalized to expression of *Gapdh* mRNA.
597 A representative image of an immunoblot from at least three independent experiments is shown.
598 Statistical significance was determined by two-way ANOVA with Bonferroni's post-hoc test
599 (A, B, C, F). *P < 0.05, ***P < 0.005, ****P < 0.001.

600

601 **Figure 3. TNF plays a role in mucosal inflammation and IEC death in LPS-treated mice**
602 **lacking linear ubiquitination activity in IECs.**

603 (A) Representative pictures (left) and quantification of colon length (right) in control and
604 HOIP^{IEC- Δ lin} mice at the indicated times after intraperitoneal administration of TNF (n=3).

605 (B) H&E staining of distal colon sections from control and HOIP^{IEC-Δlin} mice 24 h after TNF
606 treatment (n=3). Scale bars, 50 μm.

607 (C) Immunohistochemical staining for CD45 and F4/80 in distal colon sections 4 h after
608 injection of TNF (n=3). Yellow arrow heads indicate cells positive for each marker. Scale bars,
609 50 μm.

610 (D) Quantification of immune cells in (C) (n=12 fields per group).

611 (E) Immunohistochemical staining for cleaved caspase 3 in distal colon from control and
612 HOIP^{IEC-Δlin} mice 4 h after TNF treatment (n=3). Scale bars, 50 μm.

613 (F) HOIP^{IEC-Δlin} mice were injected intraperitoneally with isotype control IgG or an anti-TNF
614 antibody 1 h prior to intraperitoneal injection of LPS. Representative pictures (left) and
615 quantification of colon length (right) in isotype control- or anti-TNF-treated HOIP^{IEC-Δlin} mice
616 at the indicated times after LPS injection (n=3).

617 (G) H&E staining of the distal colon sections from isotype control- or anti-TNF-treated
618 HOIP^{IEC-Δlin} mice 24 h post-LPS administration (n=3). Scale bars, 50 μm.

619 (H) Immunohistochemical staining for CD45 and F4/80 in distal colon sections from isotype
620 control- or anti-TNF-treated HOIP^{IEC-Δlin} mice 4 h post-LPS (n=3). Yellow arrow heads depict
621 cells positive for each marker. Scale bars, 50 μm.

622 (I) Quantification of immune cells in (H) (n=12 fields per group).

623 (J) Immunohistochemical staining for cleaved caspase 3 in distal colon sections from isotype
624 control- or anti-TNF-treated HOIP^{IEC-Δlin} mice 4 h after LPS administration (n=3). Scale bars,
625 50 μm.

626 Statistical significance was determined by two-way ANOVA with Bonferroni's post-hoc test
627 (A, F), or by a two-tailed unpaired Student's t test (D, I). *P < 0.05, **P < 0.01, ****P < 0.001.

628

629 **Figure 4. Defects in epithelial linear ubiquitination activity do not overtly affect the**

630 **severity of DSS-induced colitis.**

631 (A) Control and HOIP^{IEC-Δlin} mice were fed 2.0% DSS for 7 days. They were then fed regular
632 water for 2 days. Body weight changes in control (n=7) and HOIP^{IEC-Δlin} mice (n=7) during DSS
633 treatment. BW, body weight; IBW, initial body weight.

634 (B) Representative pictures (left) and quantification of colon length (right) in DSS-treated
635 control (n=7) and HOIP^{IEC-Δlin} mice (n=7). Data from untreated control and HOIP^{IEC-Δlin} mice
636 are also shown (n=6).

637 (C) H&E staining (left) and histological damage scores (right) for distal colon sections from
638 control and HOIP^{IEC-Δlin} mice treated with DSS (n=7). Scale bars, 50 μm.

639 (D) qRT-PCR analysis of inflammatory cytokine and chemokine expression in colon tissue from
640 control (n=8) and HOIP^{IEC-Δlin} mice (n=6) subjected to DSS-induced colitis. Data from
641 untreated control and HOIP^{IEC-Δlin} mice are also shown (n=3). Data are normalized to expression
642 of *Gapdh* mRNA.

643 (E) Immunohistochemical staining for cleaved caspase 3 and immunofluorescence staining for
644 TUNEL in distal colon sections from control and HOIP^{IEC-Δlin} mice treated with DSS (n=3).
645 Yellow arrow heads depict cells positive for cleaved caspase 3. Scale bars, 50 μm.

646 Statistical significance was determined by two-way ANOVA with Bonferroni's post-hoc test
647 (A, B, D), or by a two-tailed unpaired Student's t test (C).

648

649 **Figure 5. Loss of linear ubiquitination activity in macrophages results in mild colitis after**
650 **DSS treatment.**

651 (A) Body weight changes in control (n=10) and HOIP^{MYE-Δlin} (n=13) mice during DSS treatment.

652 (B) Representative pictures (left) and quantification of colon length (right) in DSS-treated
653 control (n=8) and HOIP^{MYE-Δlin} (n=10) mice. Data from untreated control and HOIP^{MYE-Δlin} mice
654 are also shown (n=6).

655 (C) H&E staining (left) and histological damage scores (right) for distal colon from control and
656 HOIP^{MYE-Δlin} mice treated with DSS (n=5). Scale bars, 50 μm.
657 (D) Immunohistochemical staining for CD45, F4/80, B220, and CD3 in distal colon sections
658 from DSS-treated control and HOIP^{MYE-Δlin} mice (n=5). Yellow arrow heads indicate cells
659 positive for each marker. Scale bars, 50 μm.
660 (E) Quantification of immune cells in (D) (n=10 fields per group). Data from control and
661 HOIP^{MYE-Δlin} mice under basal conditions are also shown (n=6 fields per group).
662 (F) qRT-PCR analysis of inflammatory cytokine and chemokine expression in colon tissue from
663 DSS-treated control (n=5) and HOIP^{MYE-Δlin} (n=6) mice. Data from control and HOIP^{MYE-Δlin}
664 mice under basal conditions are also shown (n=3). Data are normalized to expression of *Gapdh*
665 mRNA.

666 Statistical significance was determined by two-way ANOVA with Bonferroni's post-hoc test
667 (A, B, E, F), or by a two-tailed unpaired Student's t test (C). *P < 0.05, **P < 0.01, ****P < 0.001.

668

669 **Figure 6. Deficiency of linear ubiquitination in macrophages impairs NF-κB- and ERK-**
670 **mediated inflammatory responses upon TLR stimulation.**

671 (A) BMDMs derived from control and HOIP^{MYE-Δlin} mice were stimulated with TNF (1 ng/ml)
672 for the indicated times. Cell lysates were immunoblotted with the indicated antibodies. Tubulin
673 was used as a loading control.

674 (B and C) Control and HOIP^{MYE-Δlin} BMDMs were stimulated with LPS (10 ng/ml) for the
675 indicated times. Whole cell lysates were immunoblotted with the indicated antibodies. Tubulin
676 was used as a loading control.

677 (D) BMDMs from WT mice were pre-treated with DMSO or HOIPin-8 (10 μM) for 30 min,
678 and then stimulated with LPS (10 ng/ml) for the indicated times. Whole cell lysates were
679 immunoblotted with the indicated antibodies. Tubulin was used as a loading control.

680 (E) ELISA to detect IL-6, TNF, and MCP-1/CCL2 produced by control and HOIP^{MYE-Δlin}
681 BMDMs stimulated with LPS (10 ng/ml) for 24 h (n=3).

682 (F) BMDMs from WT mice were pre-treated for 30 min with DMSO or HOIPin-8 (10 μM),
683 and then stimulated with LPS (10 ng/ml) for 24 h. Secreted IL-6, TNF, and MCP-1/CCL2 were
684 quantified by ELISA (n=3).

685 (G) BMDMs from WT mice were pre-treated with DMSO or a MEK inhibitor (0.5 μM) for 10
686 min, and then stimulated with LPS (10 ng/ml) for 24 h. Secreted IL-6, TNF, and MCP-1/CCL2
687 were quantified by ELISA (n=3).

688 (H) Control and HOIP^{MYE-Δlin} BMDMs were stimulated for 24 h with the indicated TLR ligands.
689 Secreted IL-6 was measured by ELISA (n=3). The concentrations of the TLR ligands were as
690 follows: Poly(I:C) (2 μg/ml), CpG-B (5 μM), and Pam3CSK4 (1 μg/ml).

691 A representative image of an immunoblot from at least three independent experiments is shown.
692 Statistical significance was determined by a two-tailed unpaired Student's t test (E, F, G, H).
693 *P < 0.05, **P < 0.01, ***P < 0.005, ****P < 0.001.
694

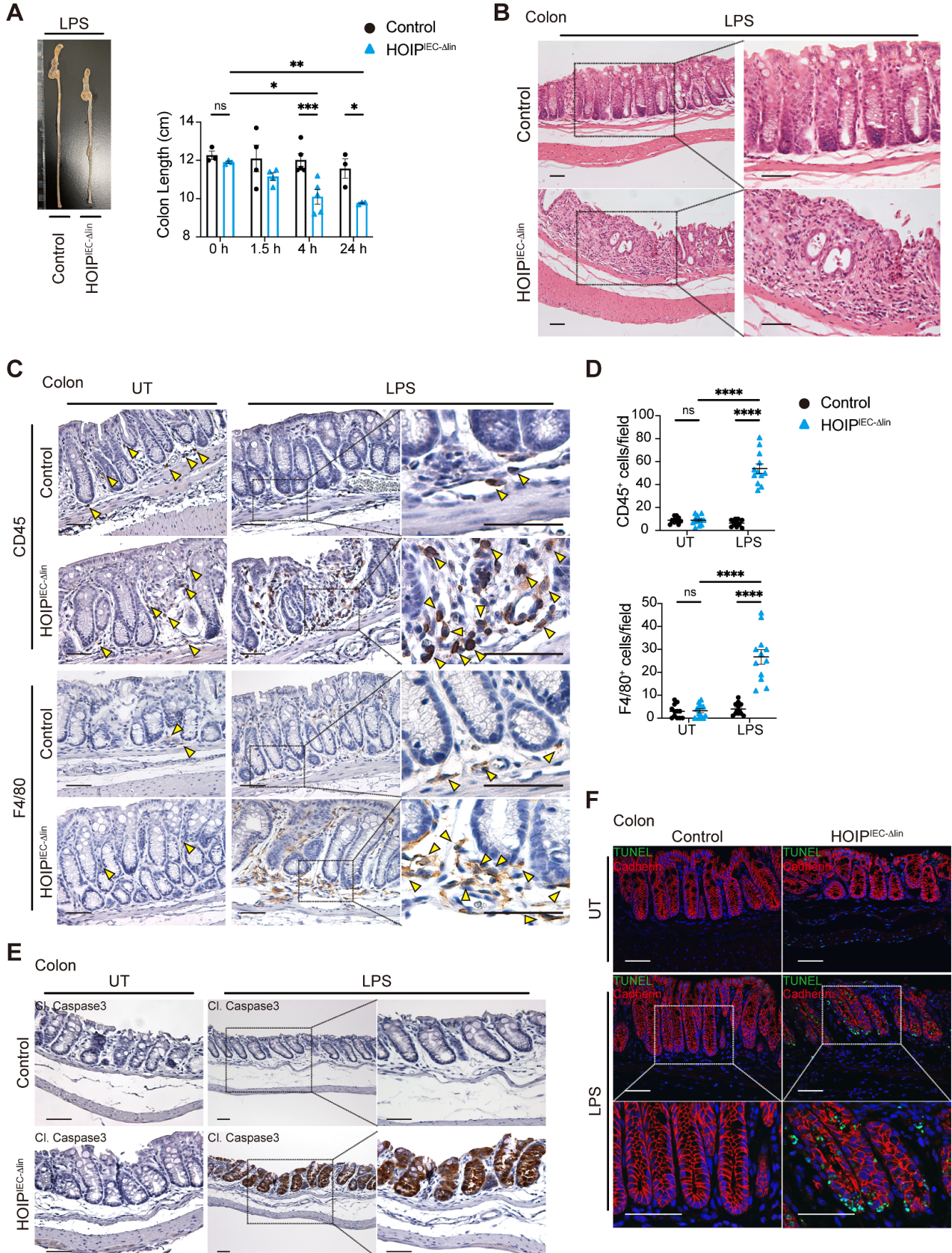


Figure 1

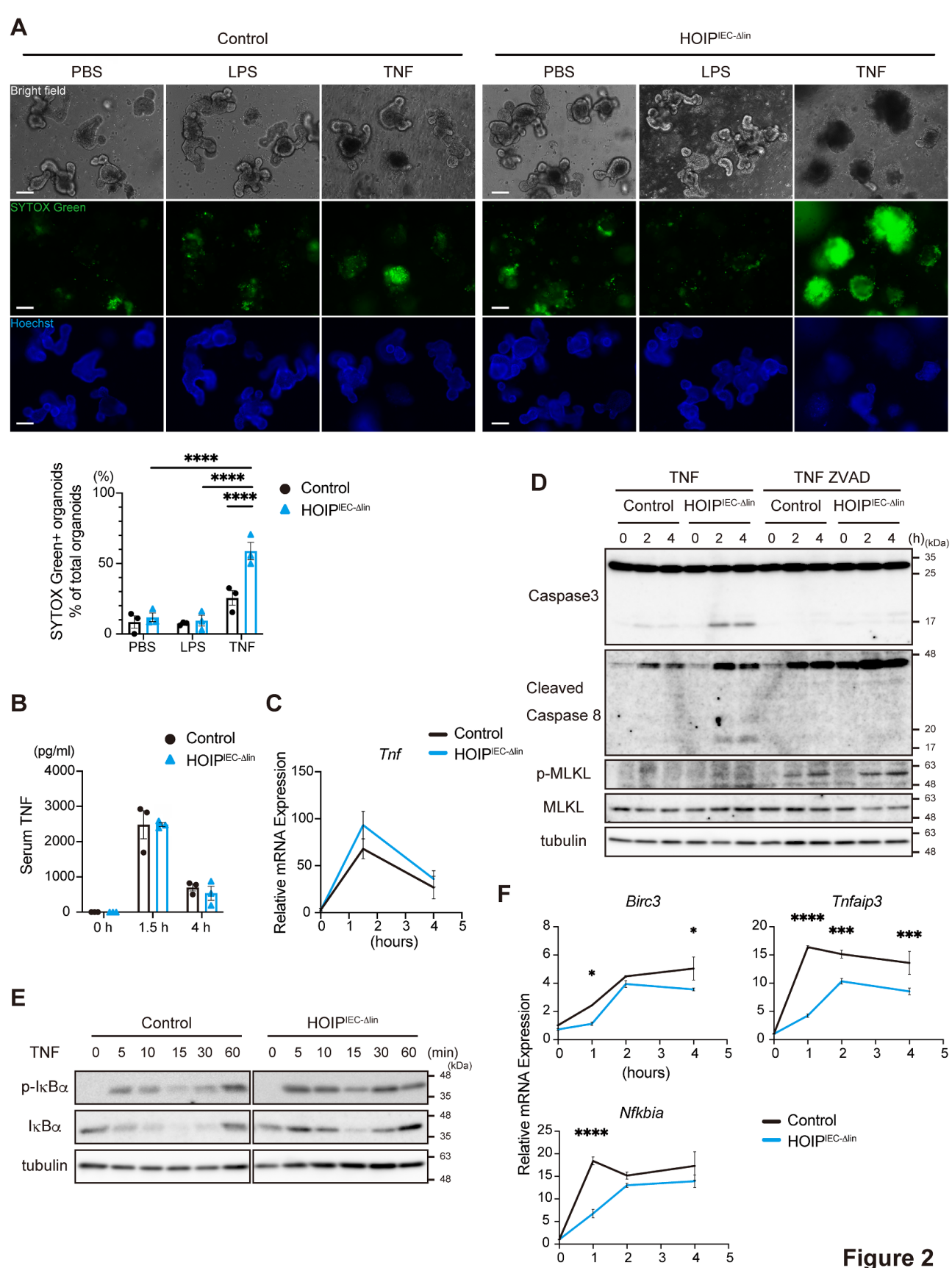


Figure 2

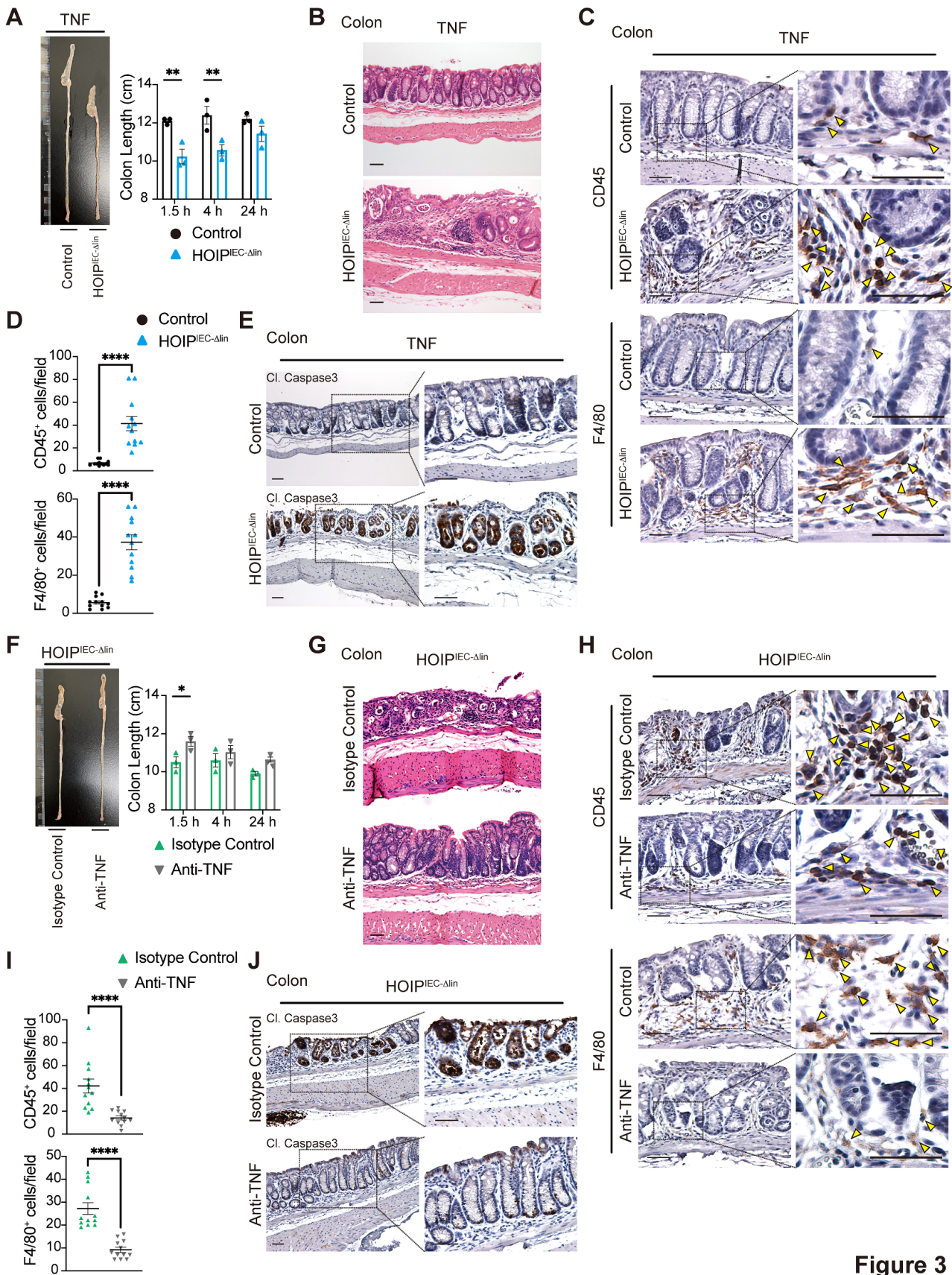


Figure 3

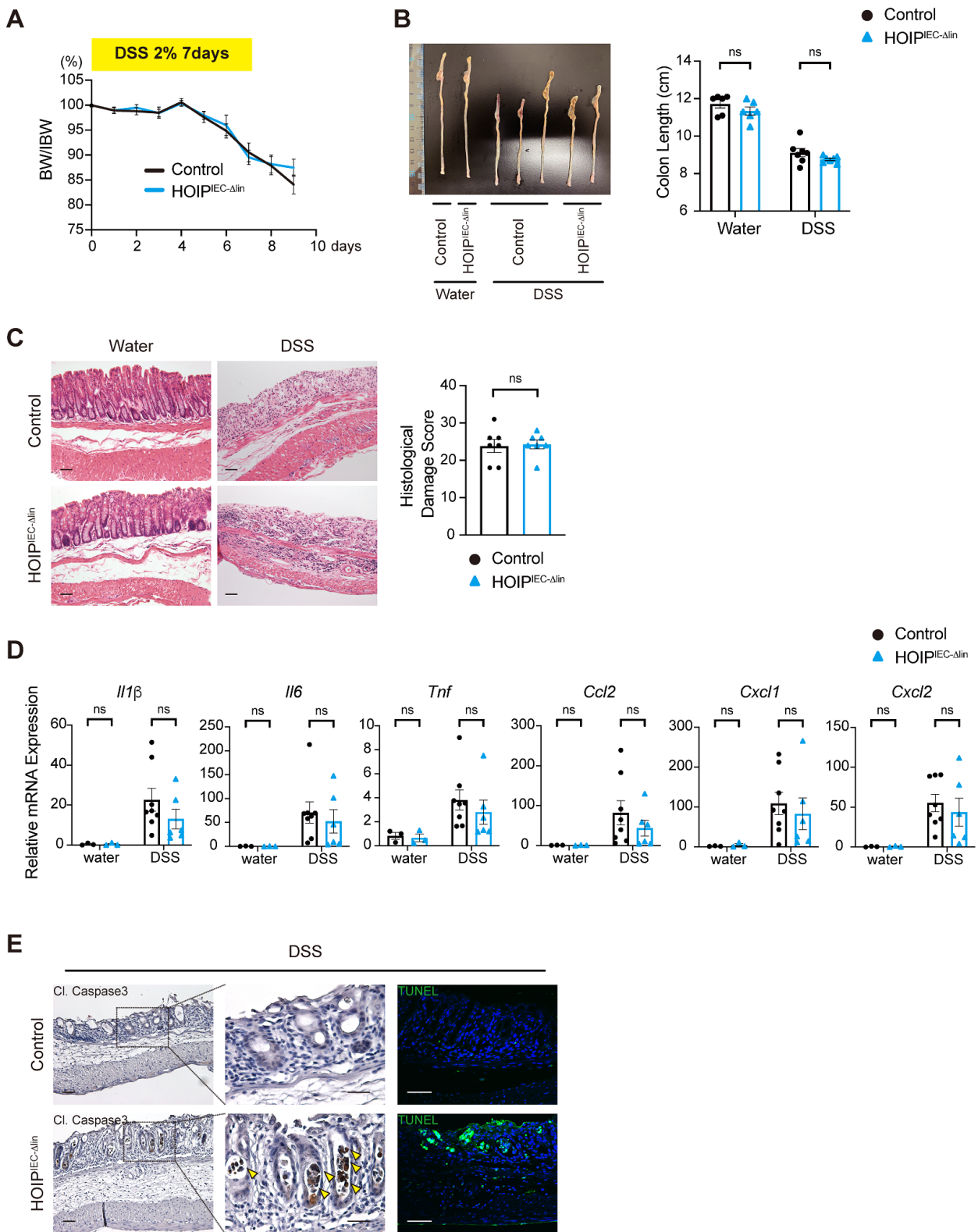


Figure 4

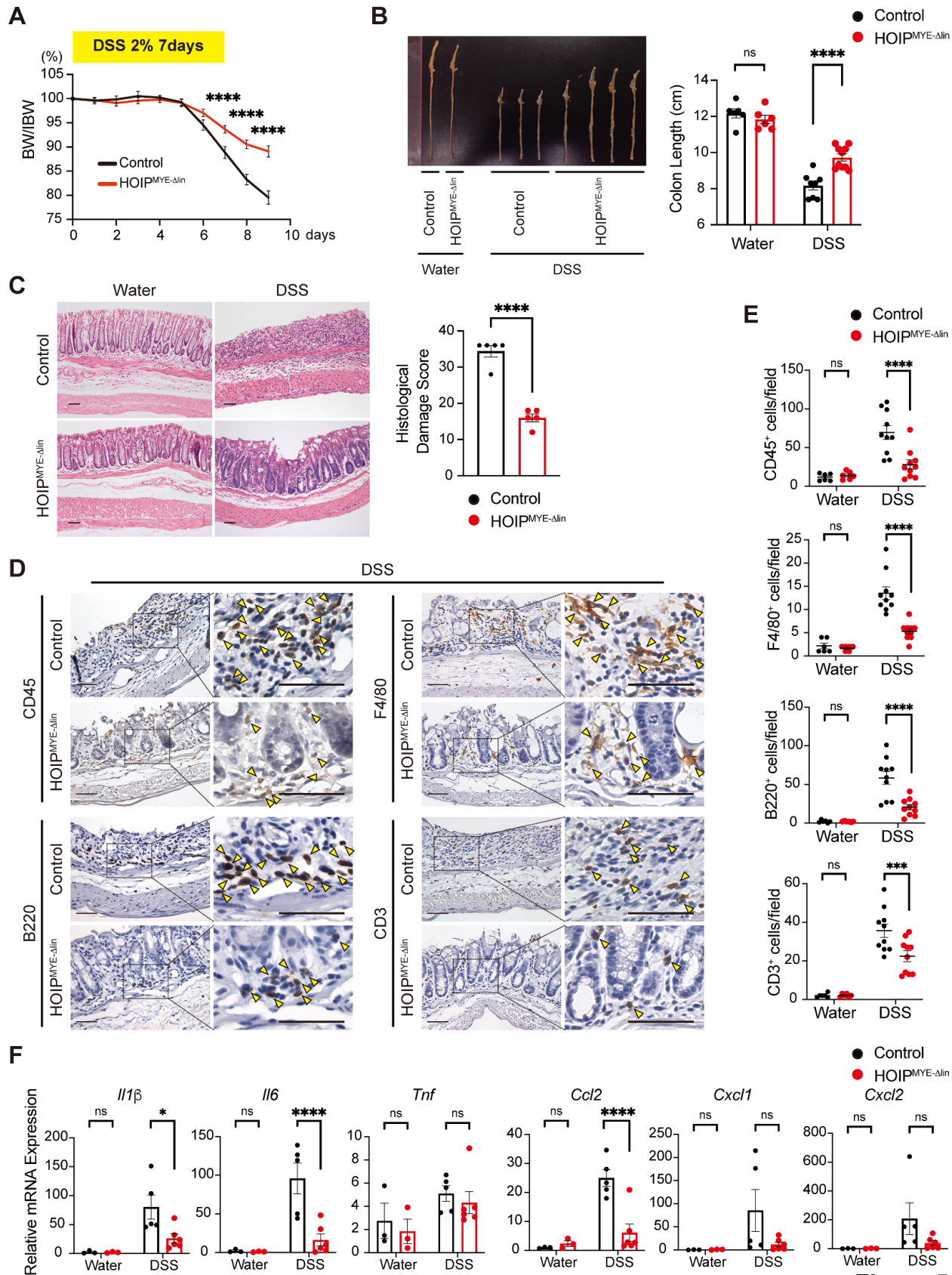


Figure 5

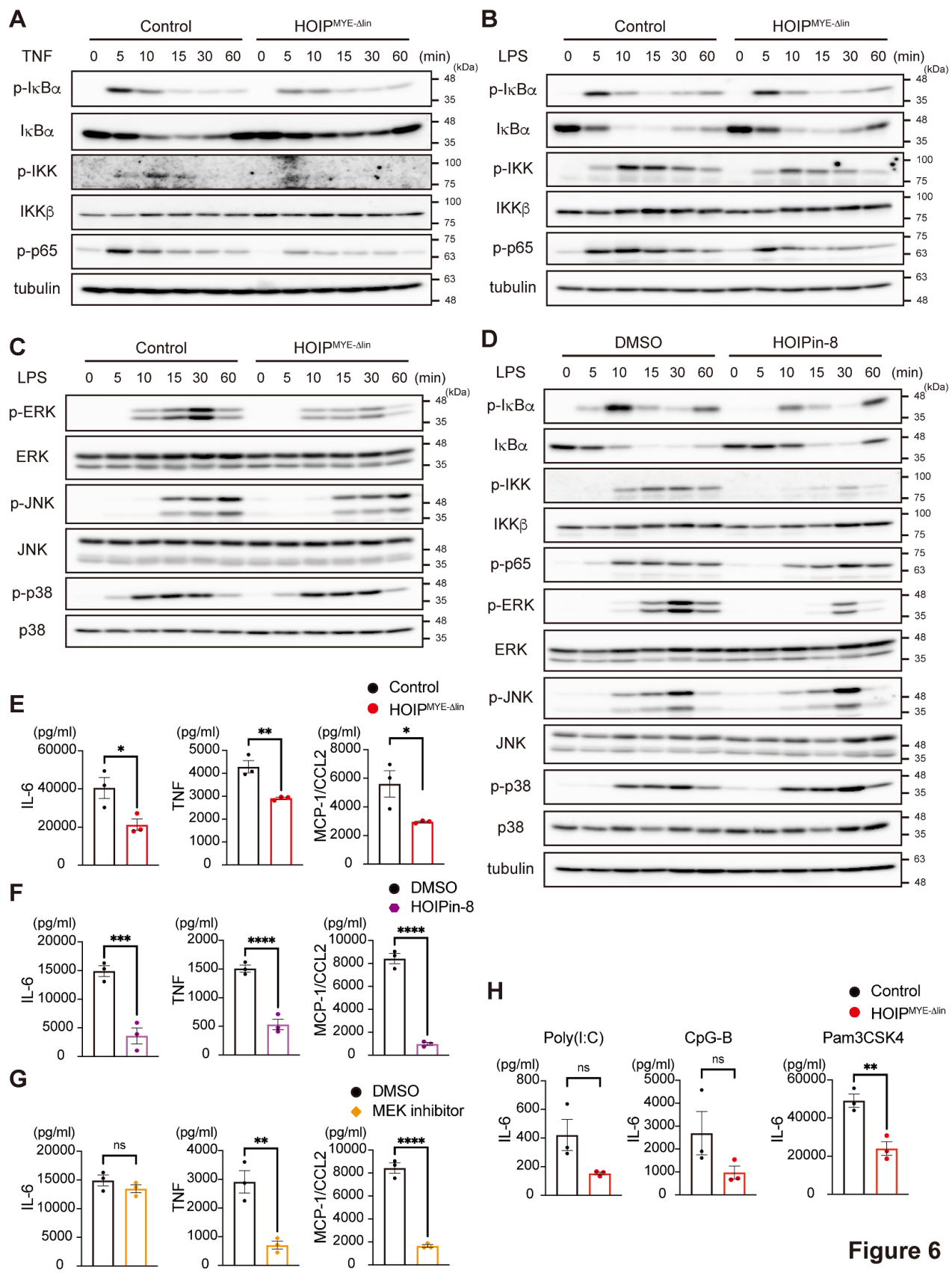


Figure 6

Supporting Information

Supplementary materials and methods

Antibodies

The following antibodies were used for immunohistochemistry: anti-CD45 (clone 30F-11, cat. no. 550539, 1:100 dilution; BD Biosciences, Franklin Lakes, NJ, USA), anti-F4/80 (clone CI:A3-1, cat. no. MCA497GA, 1:100 dilution; Bio-Rad, Hercules, CA, USA), anti-cleaved caspase-3 (cat. no. 9661, 1:100 dilution; Cell Signaling Technology, Danvers, MA, USA), anti-CD45R/B220 (clone RA3-6B2, cat. no. 103202, 1:200 dilution; BioLegend, San Diego, CA, USA), and anti-CD3 ϵ (clone M-20, cat. no. SC-1127, 1:400 dilution; Santa Cruz Biotechnology, Dallas, TX, USA). The following antibodies were used for immunofluorescence staining: anti-F4/80 (cat. no. 70076, 1:100 dilution; Cell Signaling Technology), anti-E-Cadherin (cat. no. GTX100443, 1:50 dilution; Gene Tex, Irvine, CA, USA), anti-CD3 ϵ (clone M-20, cat. no. SC-1127, 1:400 dilution; Santa Cruz Biotechnology); anti-rabbit IgG AlexaFlour 488 (cat. no. A-11034), anti-rabbit IgG-AlexaFluor 546 (cat. no. A-11035), and anti-goat IgG AlexaFlour 488 (cat. no. A-11055) (all from Invitrogen, Waltham, MA, USA; 1:200 dilution). The following antibodies were used for immunoblotting: anti-I κ B α (cat. no. 4812), anti-p-I κ B α (cat. no. 9246), anti-IKK β (cat. no. 8943), anti-p-IKK (cat. no. 2697), anti-p-p65 (cat. no. 3033), anti-ERK (cat. no. 9102), anti-p-ERK (cat. no. 9101), anti-JNK (cat. no. 9258), anti-p-JNK (cat. no. 4668), anti-p38 (cat. no. 9212), anti-p-p38 (cat. no. 9211), anti-caspase-3 (cat. no. 9662), anti-cleaved caspase-8 (cat. no. 8592) (all from Cell Signaling Technology; 1:2000 dilution); anti-MLKL (phosphor S345) (cat. no. ab196436, 1:2000 dilution; abcam, Waltham, MA, USA), anti-MLKL (cat. no. SAB1302339, 1:250 dilution; Sigma-Aldrich, St. Louis, MO, USA); anti-mouse HOIP (clone N1), anti-HOIL-1L (clone 2E2), anti-SHARPIN (clone lot1) (all produced in-house; 1:2000 dilution); β -actin (clone AC-74, cat. no. A5316, 1:5000 dilution; Sigma-Aldrich), α -tubulin

26 (clone DM1A, cat. no. CLT9002, 1:5000 dilution; CEDARLANE, Ontario, Canada),
27 HRP-linked anti-rabbit IgG (cat. no. NA934V, 1:5000 dilution; Cytiva, Marlborough, MA,
28 USA), and HRP-linked anti-mouse IgG (cat. no. 7076, Cell Signaling Technology; 1:5000
29 dilution). The following antibodies were used for flow cytometry analysis:
30 APC-Cy7-anti-CD45 (clone 30F-11, cat. no. 103116, 1:100 dilution), APC-anti-F4/80 (clone
31 BM8, cat. no. 123115, 1:200 dilution), PE-Cy7-anti-CD11b (clone M1/70, cat. no. 101215,
32 1:200 dilution), PE-Cy7-anti-CD19 (clone 6D5, cat. no. 115520, 1:200 dilution),
33 PerCP-Cy5-5-anti-CD4 (clone GK1.5, cat. no. 100434, 1:200 dilution), PE-Cy7-anti-CD8a
34 (clone 53-6.7, cat. no. 100722, 1:200 dilution), APC-anti-CD69 (clone H1.2F3, cat. no.
35 104513, 1:200 dilution), APC-anti-CD62L (clone MEL-14, cat. no. 104412, 1:200 dilution),
36 PE-anti-CD44 (clone IM7, cat. no. 103008, 1:200 dilution), streptavidin-PerCP-Cy5-5 (cat.
37 no. 405213, 1:400 dilution) (all from BioLegend); PE-anti-FAS (clone Jo2, cat. no. 554258,
38 1:200 dilution; BD Biosciences), FITC-anti-TCRb (clone H57-597, cat. no. 11-5961-82,
39 1:200 dilution; eBioscience, San Diego, CA, USA), PE-anti-CD25 (clone PC61.5, cat. no.
40 12-0251-81, 1:200 dilution, eBioscience), and Biotin-anti-PNA (cat. no. B-1075, 1:400
41 dilution, Vector Laboratories, Newark, CA, USA).

42

43 **Histological assessment of DSS-induced colitis**

44 The histological damage score was determined based on three parameters. Inflammation
45 severity was scored as 0–3, extent of inflammation was scored as 0–3, and crypt damage was
46 scored as 0–4. The sum of each parameter was multiplied by percentage involvement (0% =
47 0; $\leq 25\%$ = 1; $\leq 50\%$ = 2; $\leq 75\%$ = 3; and $\leq 100\%$ = 4) to yield the histological damage score.

48

49 **Immunostaining**

50 Immunohistochemical staining was performed using an ImmPRESS Polymer Detection Kit

51 (Vector Laboratories). Paraffin-embedded sections were deparaffinized, rehydrated, and then
52 immersed in citrate buffer (pH 6.0) for 15 min in a microwave processor (MI-77; Azumayaika,
53 Tokyo, Japan) for antigen retrieval. After blocking with normal goat or horse serum blocking
54 solution (Vector Laboratories), sections were incubated with primary antibody overnight at
55 4°C. The stained sections were incubated for 30 min at room temperature with ImmPRESS
56 Polymer Reagent (Vector Laboratories), then colored with diaminobenzidine substrate
57 (DAKO, Carpinteria, CA, USA) and counterstained with hematoxylin. Endogenous
58 peroxidase was quenched for 10 min at room temperature in 0.45% H₂O₂ in methanol or 3%
59 H₂O₂ in water. Prior to immunofluorescence staining, antigen retrieval was performed as
60 described above. After sections were blocked for 1 h with blocking buffer (2% BSA and 0.1%
61 Triton X-100 in PBS) containing 5% goat serum, sections were incubated overnight at 4°C
62 with primary antibodies diluted in blocking buffer. The stained sections were incubated for 1
63 h at room temperature with fluorescent dye-conjugated anti-rabbit IgG-AlexaFluor 488 or
64 anti-goat IgG-AlexaFluor 488 in blocking buffer. For preservation, labeled sections were
65 mounted in ProLong Glass Antifade Mountant (Invitrogen). TUNEL staining was performed
66 using an In Situ Cell Death Detection Kit, Fluorescein (Sigma-Aldrich). Prior to co-staining
67 for TUNEL and for E-Cadherin, antigen retrieval was performed as described above. Then,
68 sections were incubated for 1 h at 37°C with TUNEL reaction mixture. After blocking as
69 described above, sections were incubated overnight at 4°C with an anti-E-Cadherin antibody
70 in blocking buffer. The stained sections were then incubated for 1 h at room temperature with
71 fluorescent dye-conjugated anti-rabbit IgG-AlexaFluor 546 in blocking buffer. For
72 preservation, labeled sections were mounted in ProLong Glass Antifade Mountant
73 (Invitrogen). DAPI was used to stain nuclei.

74

75 **IEC isolation and organoid culture**

76 The distal 10 cm segment of the small intestine or the whole colon was opened longitudinally
77 and minced. The intestinal segments were washed with cold PBS and incubated at 4°C for 40
78 min with PBS containing 5 mM EDTA and 10% FBS (whole colon was incubated for 60 min)
79 with rocking. After removal of the EDTA medium, the tissue fragments were shaken
80 vigorously in cold PBS to detach the villous and crypt fractions, and then passed through a
81 100 µm cell strainer (Corning, Glendale, AZ, USA). For IEC isolation, the flow-through were
82 pelleted and lysed for RNA extraction or immunoblotting. For organoid culture, the
83 flow-through from the small intestine was filtered through a 70 µm cell strainer (Corning) to
84 remove villous material. Isolated crypts were mixed with 50 µl of Matrigel (Corning) and
85 plated in 24-well plates. After the Matrigel polymerized, 500 µl of IntestiCult Organoid
86 Growth Medium (STEMCELL Technologies, Vancouver, Canada) was added to each well,
87 followed by cultivation at 37°C/5% CO₂.

88

89 **Enrichment of peritoneal macrophages**

90 Peritoneal macrophages were obtained by flushing out the peritoneal cavity with 10 ml of
91 cold PBS. The collected medium was plated into 6 or 12 well plates for 2 h. Non-adherent
92 cells were washed away with PBS and the attached cells were used as peritoneal macrophages.
93 Primary cells from each organ were washed with Gey's Buffer to deplete red blood cells.

94

95 **Immunoblotting**

96 Cells were lysed with lysis buffer containing 50 mM Tris-HCl (pH 7.5), 150 mM NaCl, 1%
97 Triton X-100, 2 mM PMSF, and protease inhibitor cocktail (Sigma-Aldrich). **Organoids were**
98 **lysed in RIPA buffer (50 mM Tris-HCl (pH 8.0), 150 mM NaCl, 1% Triton X-100, 0.1% SDS,**
99 **0.1% sodium deoxycholate, 2 mM PMSF, and protease inhibitor cocktail; (Sigma-Aldrich)).**
100 Lysates were centrifuged at 15,000 rpm for 10 min at 4°C, and the supernatant was used in

101 subsequent steps. To examine phosphorylation, a phosphatase inhibitor cocktail (Nacalai
102 Tesque, Kyoto, Japan) was added. To assess the protein translocating to the nucleus, total cell
103 lysates were obtained by incubation in SDS sample buffer. The cell lysates were then
104 separated by SDS-PAGE and transferred onto PVDF membranes (Merck Millipore,
105 Burlington, MA, USA). After blocking in Tris-buffered saline containing 0.1% Tween 20 and
106 5% nonfat dry milk, the membrane was immunoblotted with the indicated primary antibodies,
107 followed by the corresponding secondary antibodies. The membranes were visualized by
108 enhanced chemiluminescence and analyzed by an LAS3000 or LAS4000mini instrument (GE
109 Healthcare, Chicago, IL, USA).

110

111 **Quantitative RT-PCR analysis**

112 Total RNA from IECs or organoids was extracted using an RNeasy Mini Kit (Qiagen, Venlo,
113 Netherlands). To extract RNA from colon tissue, 5 mm segments taken from between the
114 middle and distal third of the colon were used. Pre-purified RNAs were extracted using
115 ISOGEN (NIPPON GENE, Tokyo, Japan), and then subjected to column-based purification
116 using an RNeasy Mini Kit (Qiagen). Total RNA was reverse transcribed into cDNA using a
117 High Capacity RNA-to-cDNA Kit ([Thermo Fisher Scientific](#)). Real-time PCR was performed
118 with Power SYBR Green PCR Master Mix (Thermo Fisher Scientific) and a ViiA7 Real-Time
119 PCR system (Applied Biosystems, Waltham, MA, USA). The results were analyzed by the
120 $\Delta\Delta$ CT method. The sequences of the primers used for qPCR are listed in Table S1.

121

122 **ELISA**

123 Cell culture supernatants and serum were collected and stored at -80°C until use. The
124 concentrations of [TNF](#), IL-6, and MCP-1/CCL2 in culture supernatants and serum were
125 measured using an ELISA MAX Standard Set (BioLegend). BD OPtEIA (BD Biosciences)

126 was used as the substrate. Absorbance at 450 nm, with a correction wave length of 570 nm,
127 was detected by a microplate reader (Molecular Devices, San Jose, CA, USA).

128

129 Flow cytometry

130 Primary cells isolated from the spleen or peripheral lymph nodes, or BMDMs, were incubated
131 with a mixture of the fluorochrome-conjugated antibodies. Samples were run on FACSCanto
132 II (BD Biosciences) using FACS Diva software v.6.1.2 (BD Biosciences). The results were
133 analyzed using FlowJo software v.9.9.6 (Tomy Digital Biology, Tokyo, Japan).

134

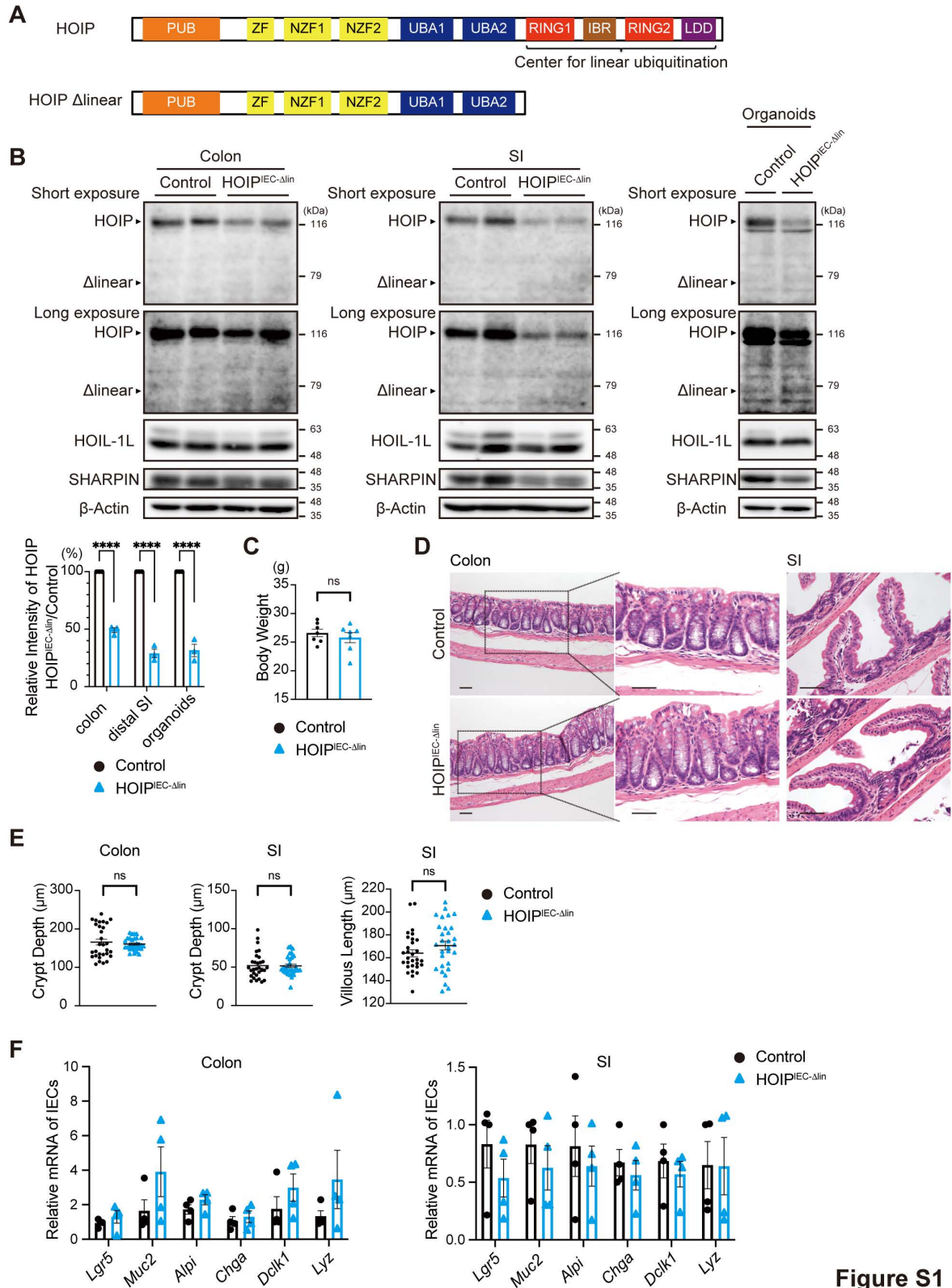


Figure S1

136

137 **Figure S1. No morphological or developmental changes in the intestine of HOIP^{IEC-Δlin}**

138 **mice under basal conditions.**

139 (A) Schematic illustration of the target region within the HOIP gene.

140 (B) Immunoblot analysis (top) of LUBAC subunits in lysates of IECs from the colon and the
141 small intestine (SI) and organoids of control and HOIP^{IEC-Δlin} mice. β-actin was used as a
142 loading control. Relative band intensity (bottom) of HOIP in HOIP^{IEC-Δlin} mice, normalized to
143 the intensity in littermate controls (n=3).

144 (C) Body weight of control and HOIP^{IEC-Δlin} mice under basal conditions (n=7). ns, not
145 significant.

146 (D) H&E staining of the colon and the small intestine from control and HOIP^{IEC-Δlin} mice
147 (n=3). Scale bars, 50 μm.

148 (E) Crypt length in the colon and small intestine, and villous length in the small intestine, of
149 control and HOIP^{IEC-Δlin} mice (n=30 fields per group).

150 (F) qRT-PCR analysis of expression of mRNA encoding epithelial markers by IECs from the
151 colon and small intestine of control and HOIP^{IEC-Δlin} mice (n=4). Data are normalized to
152 expression of *Gapdh* mRNA.

153 Statistical significance was determined by two-way ANOVA with Bonferroni's post-hoc test
154 (B, F) or a two-tailed unpaired Student's t test (C, E). ****P < 0.001.

155

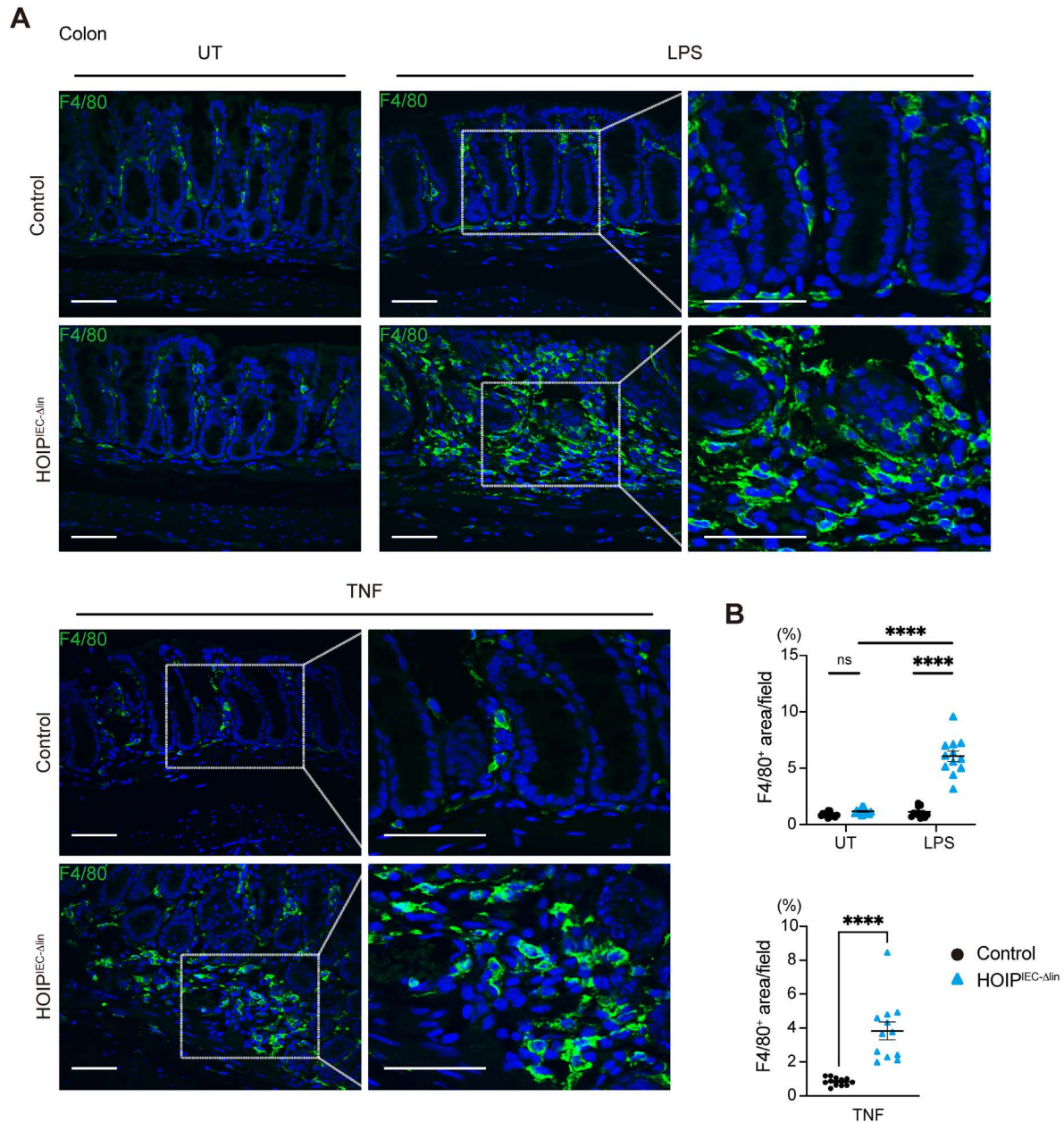


Figure S2

156

157 **Figure S2. Immunofluorescence staining for F4/80 in distal colon sections from control**
 158 **and HOIP^{IEC-Δlin} mice after injection of LPS or TNF.**

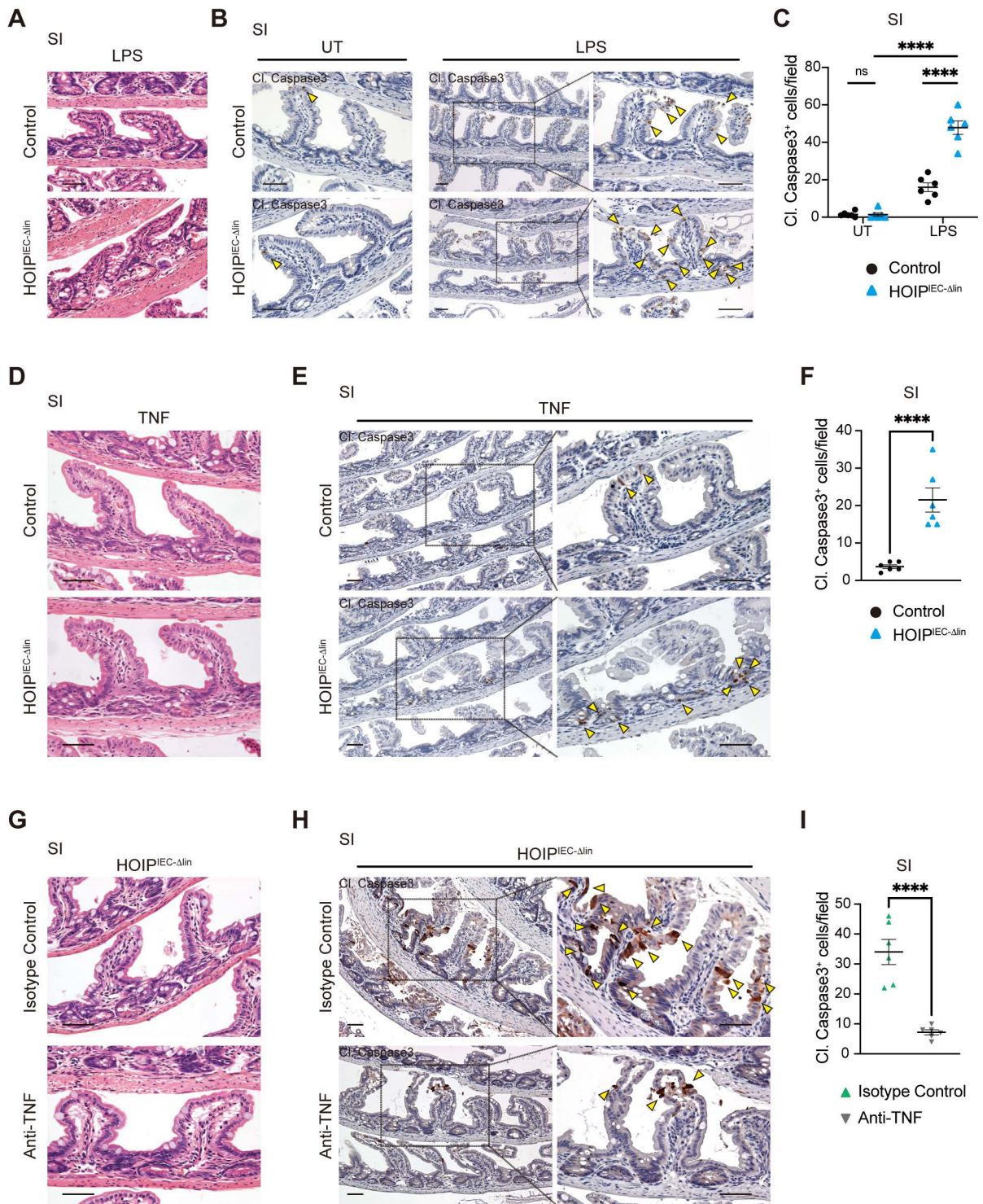
159 (A) Immunofluorescence staining for F4/80 in the distal colon 4 h post-injection of LPS or
 160 TNF (n=3). Data from untreated control (UT) and HOIP^{IEC-Δlin} mice are also shown (n=3).
 161 Scale bars, 50 μm.

162 (B) Quantification of the F4/80⁺ cells in (A) (n=12 fields per group).

163 Statistical significance was determined by two-way ANOVA with Bonferroni's post-hoc

164 test (B, top), or a two-tailed unpaired Student's t test (B, bottom). **** $P < 0.001$.

165



166

Figure S3

167 **Figure S3. TNF mediates IEC death in the small intestine of HOIP^{IEC-Δlin} mice upon LPS**
168 **administration.**

169 (A) H&E staining of small intestine sections from control and HOIP^{IEC-Δlin} mice 24 h after
170 LPS administration (n=3). Scale bars, 50 μm.

171 (B) Immunohistochemical staining of cleaved caspase 3 (Cl. Caspase3) in sections of small
172 intestine at 1.5 h post-LPS treatment (n=3). Data of untreated control and HOIP^{IEC-Δlin} mice
173 are also shown (n=3). Yellow arrow heads show cells positive for cleaved caspase 3 in the
174 small intestine. Scale bars, 50 μm.

175 (C) Number of cleaved caspase 3-positive cells in the small intestine (n=6 fields per group).

176 (D) H&E staining of small intestine sections from control and HOIP^{IEC-Δlin} mice 24 h after
177 TNF treatment (n=3). Scale bars, 50 μm.

178 (E) Immunohistochemical staining of cleaved caspase 3 in the small intestine of control and
179 HOIP^{IEC-Δlin} mice 1.5 h post-TNF treatment (n=3). Yellow arrow heads show cells positive for
180 cleaved caspase 3. Scale bars, 50 μm.

181 (F) Number of cleaved caspase 3-positive cells in the small intestine (n=6 fields per group).

182 (G) H&E staining of the small intestine sections from isotype control- or anti-TNF-treated
183 HOIP^{IEC-Δlin} mice 24 h post-LPS administration (n=3). Scale bars, 50 μm.

184 (H) Immunohistochemical staining for cleaved caspase 3 in the small intestine of isotype
185 control- or anti-TNF-treated HOIP^{IEC-Δlin} mice 1.5 h post-LPS administration (n=3). Yellow
186 arrow heads show cells positive for cleaved caspase 3. Scale bars, 50 μm.

187 (I) Number of cleaved caspase 3-positive cells in the small intestine (n=6 fields per group).

188 Statistical significance was determined by two-way ANOVA with Bonferroni's post-hoc test

189 (C), or a two-tailed unpaired Student's t test (F, I). ****P < 0.001.

190

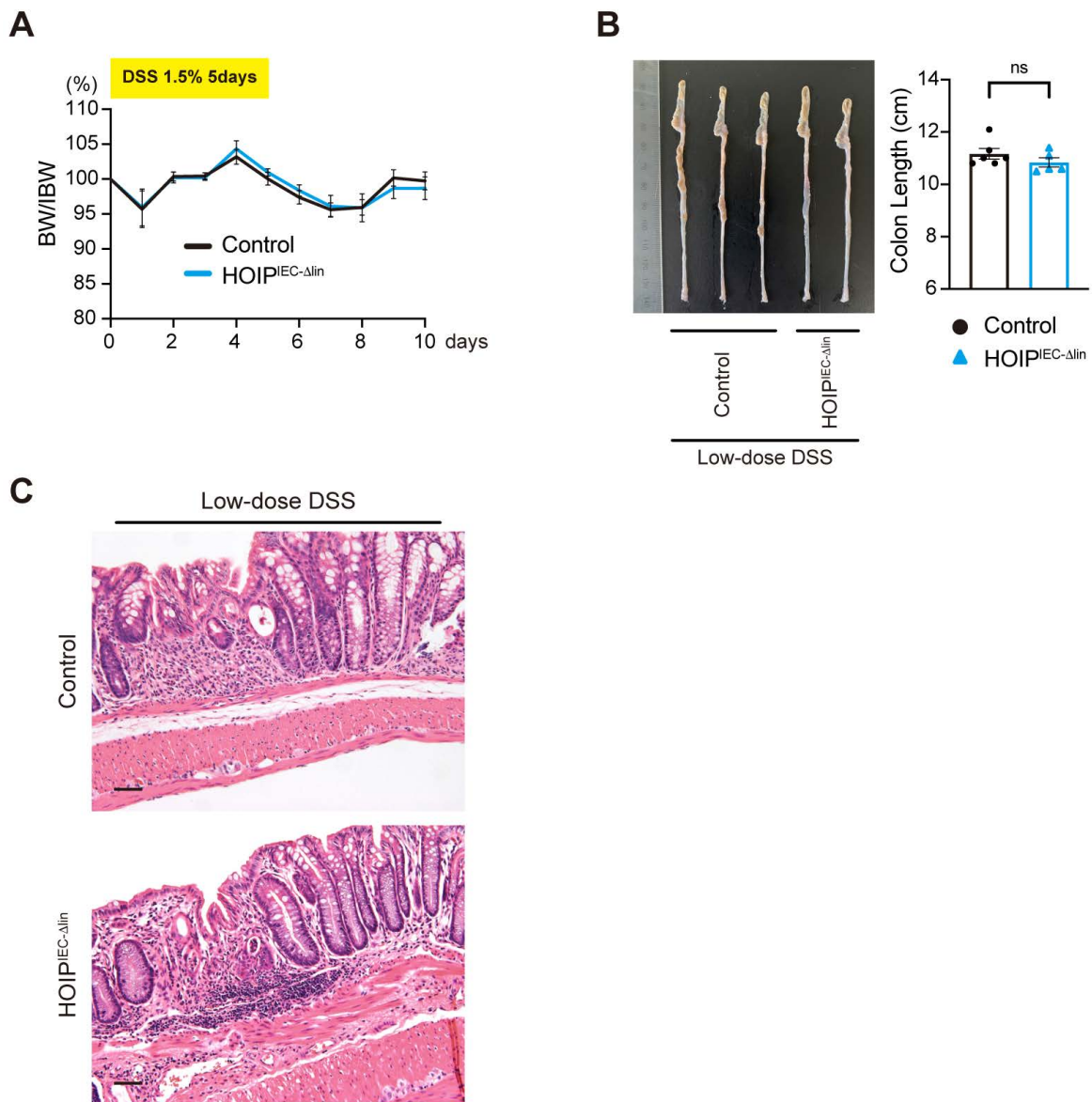


Figure S4

191

192 **Figure S4. Loss of linear ubiquitination activity in IECs does not overtly affect the**
 193 **severity of low-dose DSS-induced colitis.**

194 (A) Control and HOIP^{IEC-Δlin} mice were fed 1.5% DSS for 5 days. They were then fed regular
 195 water for 5 days. Body weight changes in control (n=6) and HOIP^{IEC-Δlin} mice (n=5) were
 196 measured during DSS treatment. BW, body weight; IBW, initial body weight.

197 (B) Representative pictures (left) and quantification of colon length (right) in DSS-treated
 198 control (n=6) and HOIP^{IEC-Δlin} mice (n=5).

199 (C) H&E staining of distal colon sections from control and HOIP^{IEC-Δlin} mice treated with

200 DSS (n=5). Scale bars, 50 μ m.

201 Statistical significance was determined by two-way ANOVA with Bonferroni's post-hoc test

202 (A), or by a two-tailed unpaired Student's t test (B).

203

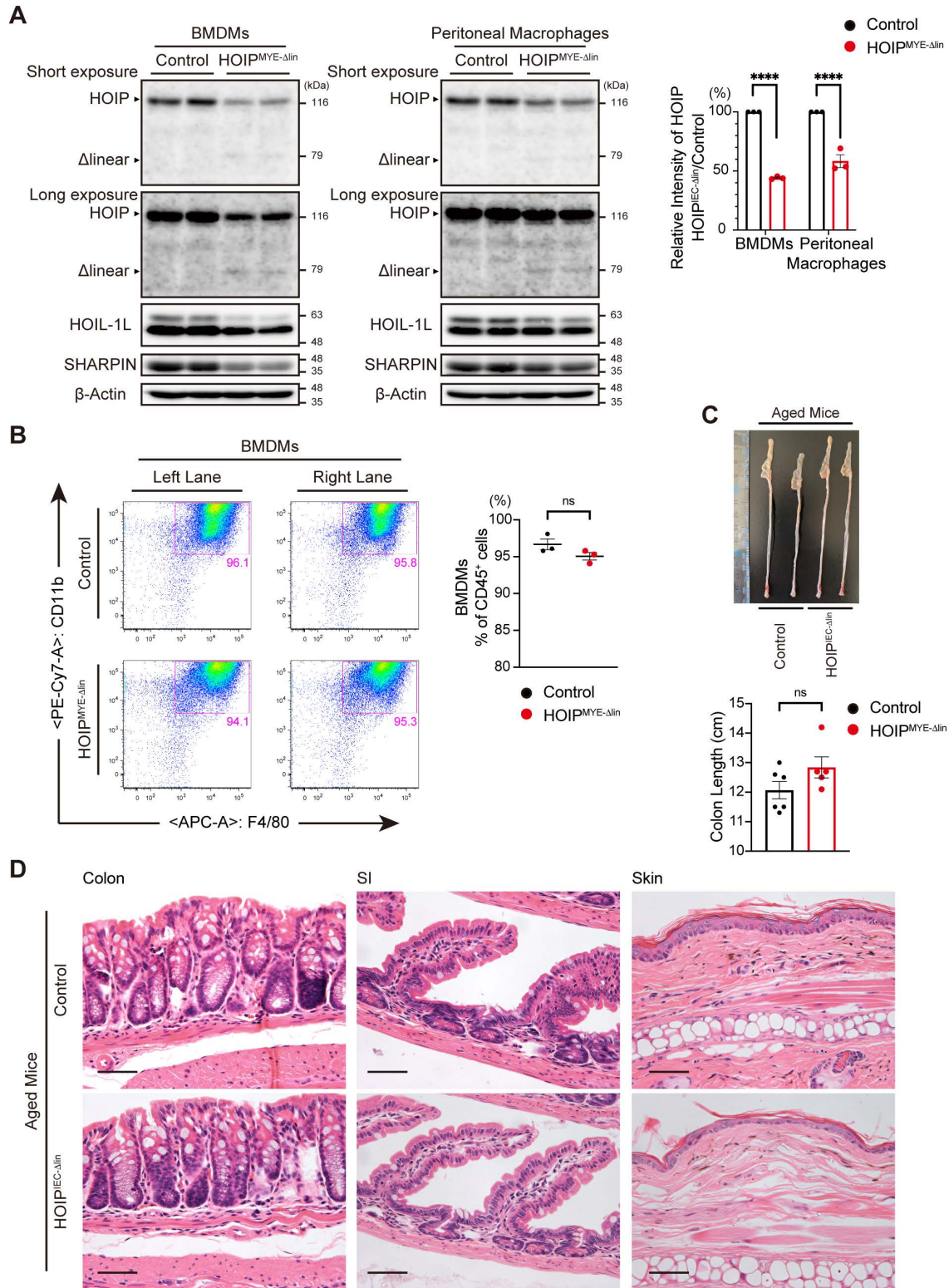


Figure S5

204

205 **Figure S5. Aged HOIP^{MYE-Δlin} mice do not show inflammatory or autoimmune**
 206 **phenotypes under basal conditions.**

207 (A) Immunoblot analysis (left) of LUBAC subunits in lysates of BMDMs and peritoneal

208 macrophages from control and HOIP^{MYE-Δlin} mice. β-actin was used as a loading control.
209 Relative band intensity (right) of HOIP in HOIP^{IEC-Δlin} mice, normalized to the intensity in
210 littermate controls (n=3).
211 (B) Flow cytometry analysis of BMDM differentiation in (A) (left), and the proportion of
212 differentiated BMDMs (F4/80⁺CD11b⁺) among CD45⁺ cells (n=3) (right).
213 (C) Representative pictures (top), and quantification of colon length (bottom), from aged
214 control (n=6) and HOIP^{MYE-Δlin} mice (n=5). Aged mice were 24–32 weeks old.
215 (D) H&E staining of the colon, small intestine, and skin from aged control and HOIP^{MYE-Δlin}
216 mice (n=3). Scale bars, 50 μm.
217 Statistical significance was determined by two-way ANOVA with Bonferroni's post hoc-test
218 (A) or a two-tailed unpaired Student's t test (B, C). ****P < 0.001.
219

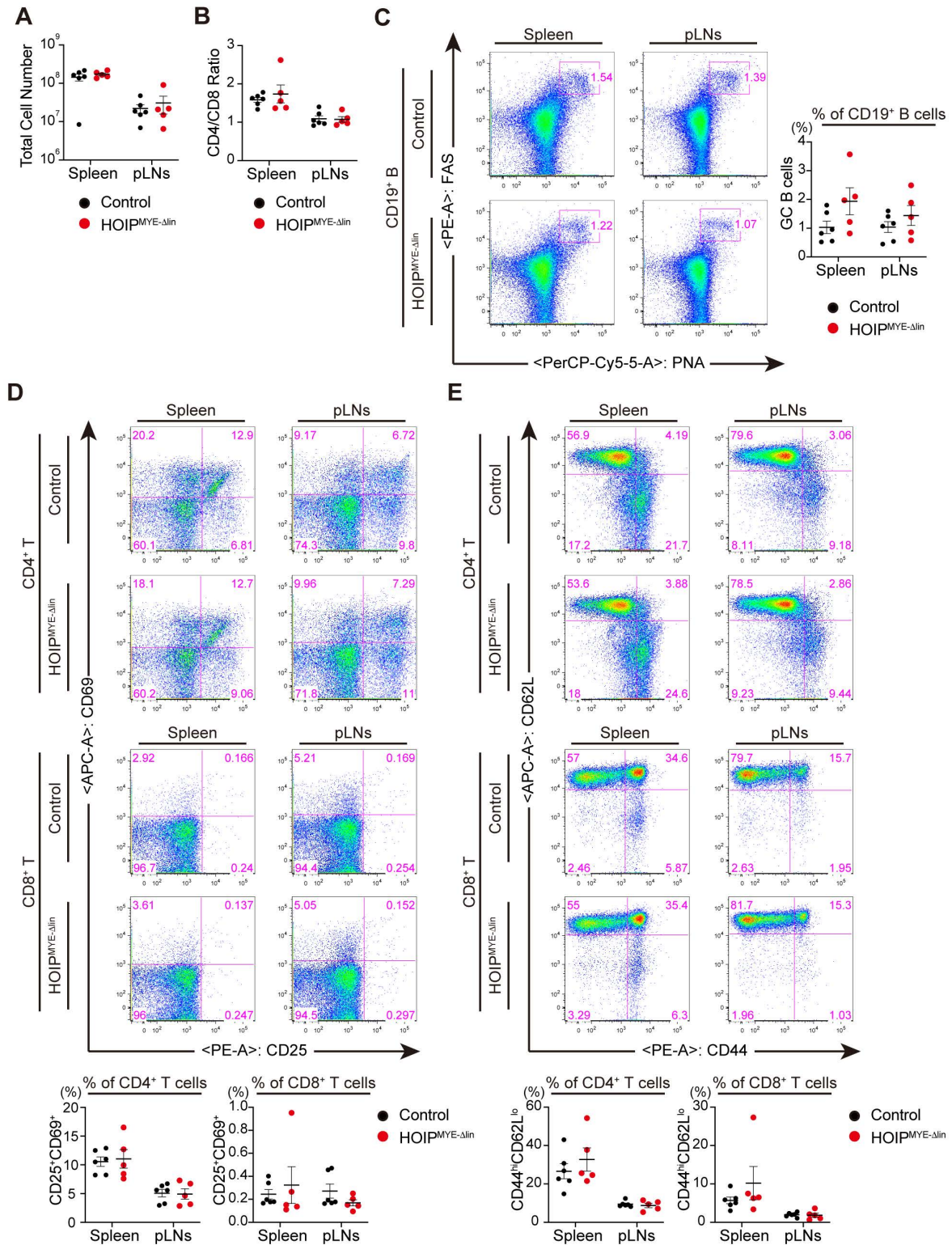


Figure S6

220

221 **Figure S6. No overt changes in the proportion of activated lymphocytes in aged**

222 **HOIP^{MYE-Δlin} mice under basal conditions.**

223 **(A) Total number of immune cells in the spleen and peripheral lymph nodes (pLNs) from**

224 aged control (n=6) and HOIP^{MYE-Δlin} mice (n=5).

225 (B) Flow cytometry analysis of the CD4/CD8 T cell ratio in aged control (n=6) and
226 HOIP^{MYE-Δlin} mice (n=5).

227 (C) Representative flow cytometry plots (left) and percentages (right) of germinal center (GC)
228 B cells (PNA⁺FAS⁺) within the CD19⁺ B cell population in the spleen and pLNs of aged
229 control (n=6) and HOIP^{MYE-Δlin} mice (n=5).

230 (D) Representative flow cytometry plots (top) and percentages (bottom) of activated T cells
231 (CD25⁺CD69⁺) in the CD4⁺ and CD8⁺ T cell populations in the spleen and pLNs of aged
232 control (n=6) and HOIP^{MYE-Δlin} mice (n=5).

233 (E) Representative flow cytometry data (top) and percentages (bottom) of effector T cells
234 (CD44^{hi}CD62L^{lo}) in the CD4⁺ and CD8⁺ T cell populations in the spleen and pLNs of aged
235 control (n=6) and HOIP^{MYE-Δlin} mice (n=5).

236 Statistical significance was determined by two-way ANOVA with Bonferroni's post hoc-test
237 (A–E).

238

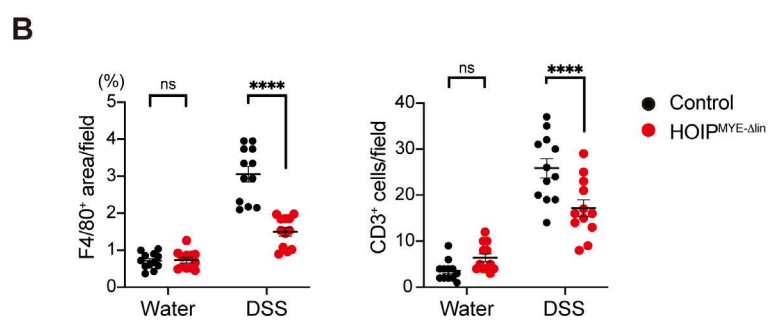
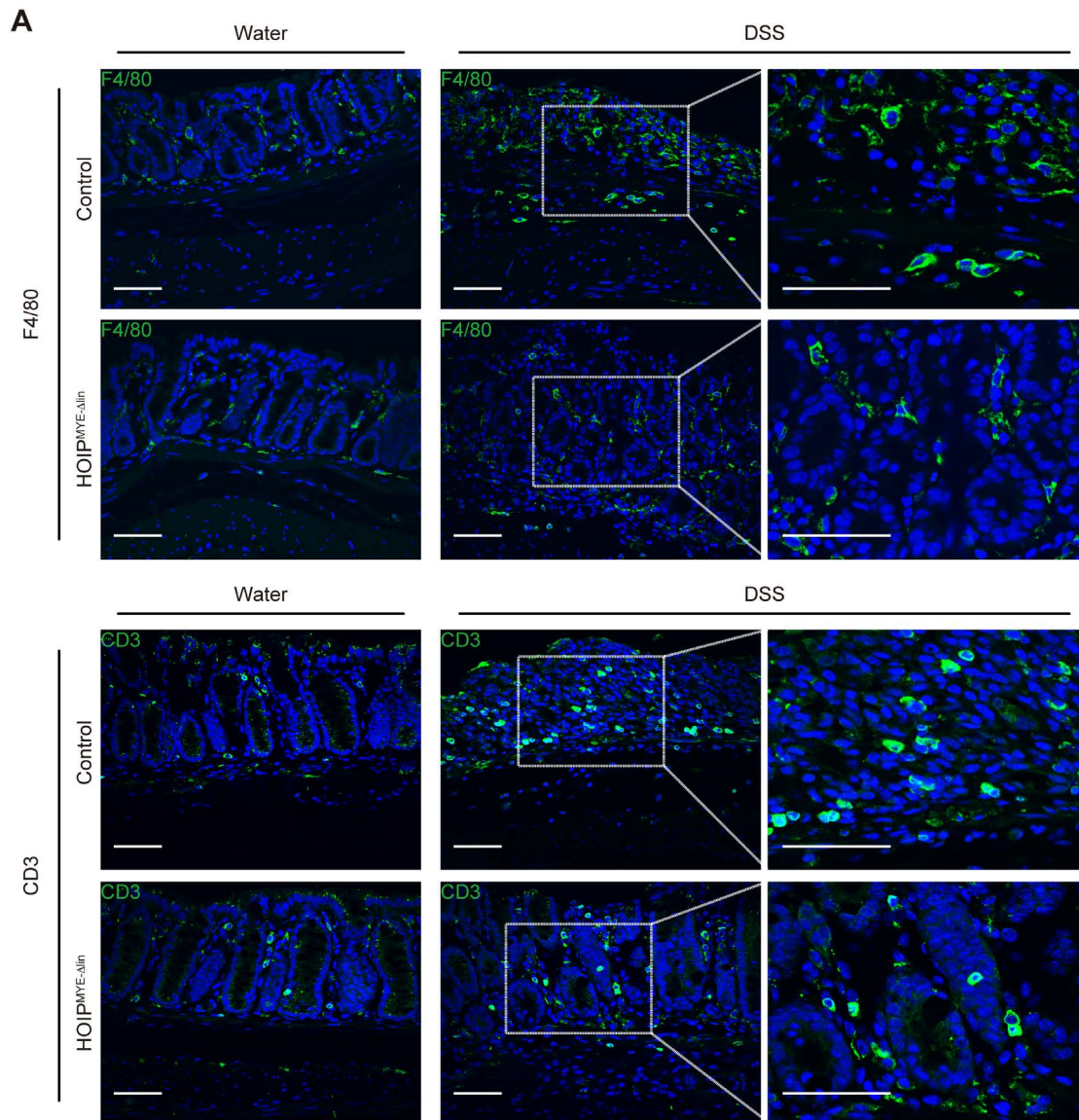


Figure S7

239

240 **Figure S7. Immunofluorescence staining of F4/80 and CD3 in distal colon sections from**
 241 **DSS-treated control and HOIP^{MYE-Δlin} mice.**

242 (A) Immunofluorescence staining for F4/80 and CD3 in distal colon sections from
 243 DSS-treated control and HOIP^{MYE-Δlin} mice (n=3). Data from untreated control and

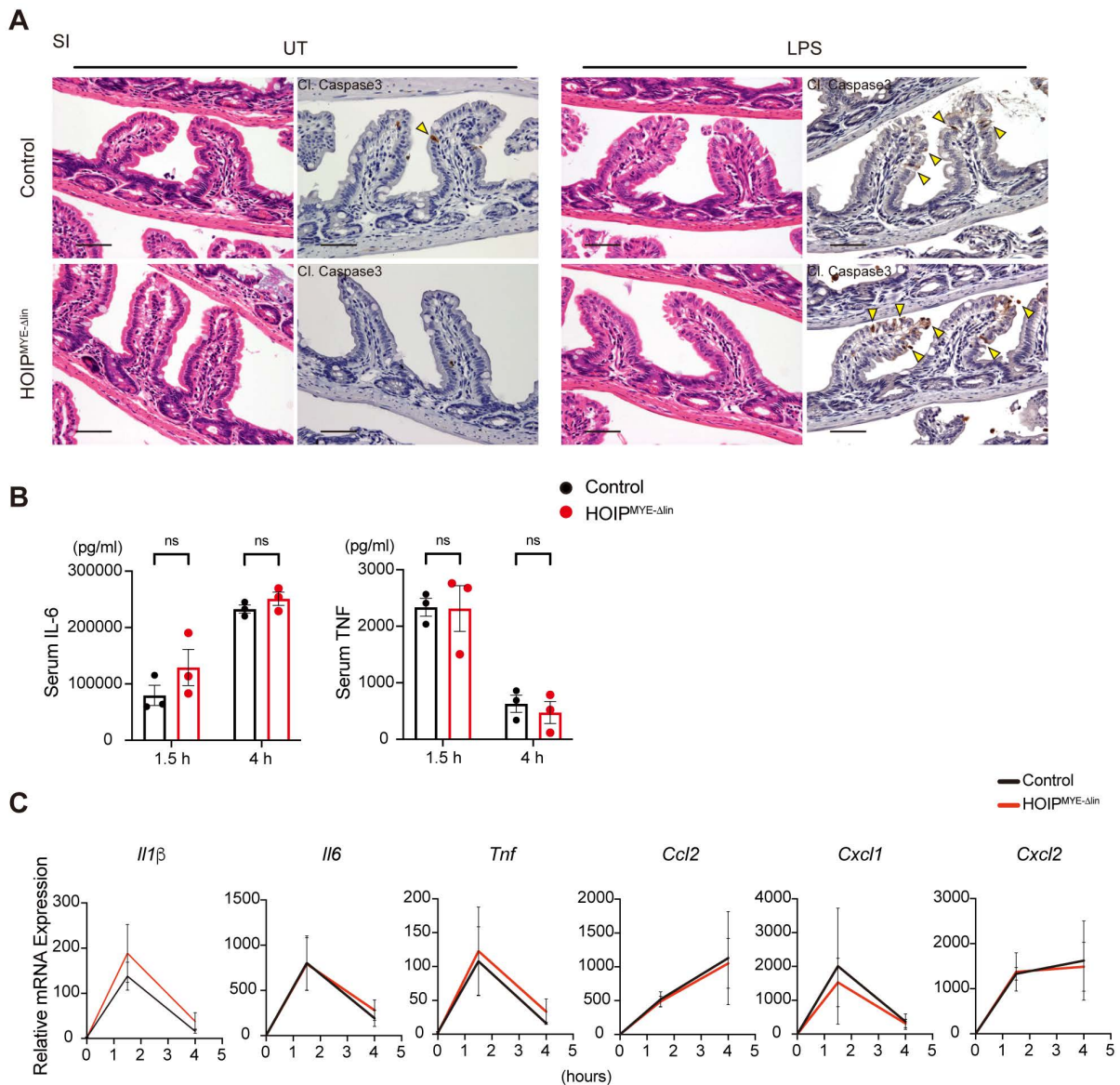
244 HOIP^{MYE-Δlin} mice are also shown (n=3). Scale bars, 50 μm.

245 (B) Quantification of immune cells in (A) (n=12 fields per group).

246 Statistical significance was determined by two-way ANOVA with Bonferroni's post hoc-test

247 (B).

248



249

Figure S8

250 **Figure S8. Attenuation of LUBAC ligase activity in macrophages has no effect in an**
251 **LPS-induced IEC shedding model.**

252 (A) H&E staining and immunohistochemical staining of small intestine sections for cleaved

253 caspase 3 at 1.5 h post-intraperitoneal administration of LPS to control and HOIP^{MYE-Δlin} mice
254 (n=3). Data from **untreated control** and HOIP^{MYE-Δlin} mice are also shown (n=3). Yellow
255 arrows head indicate cells positive for cleaved caspase 3. Scale bars, 50 μm.

256 **(B)** ELISA used to measure serum IL-6 and **TNF** levels in control and HOIP^{MYE-Δlin} mice after
257 LPS injection (n=3).

258 **(C)** qRT-PCR analysis of inflammatory cytokine and chemokine expression in colon tissue
259 from LPS-treated control and HOIP^{MYE-Δlin} mice (n=3). Data are normalized to expression of
260 *Gapdh* mRNA.

261 Statistical significance was determined by two-way ANOVA with Bonferroni's post-hoc test
262 **(B, C)**.

263

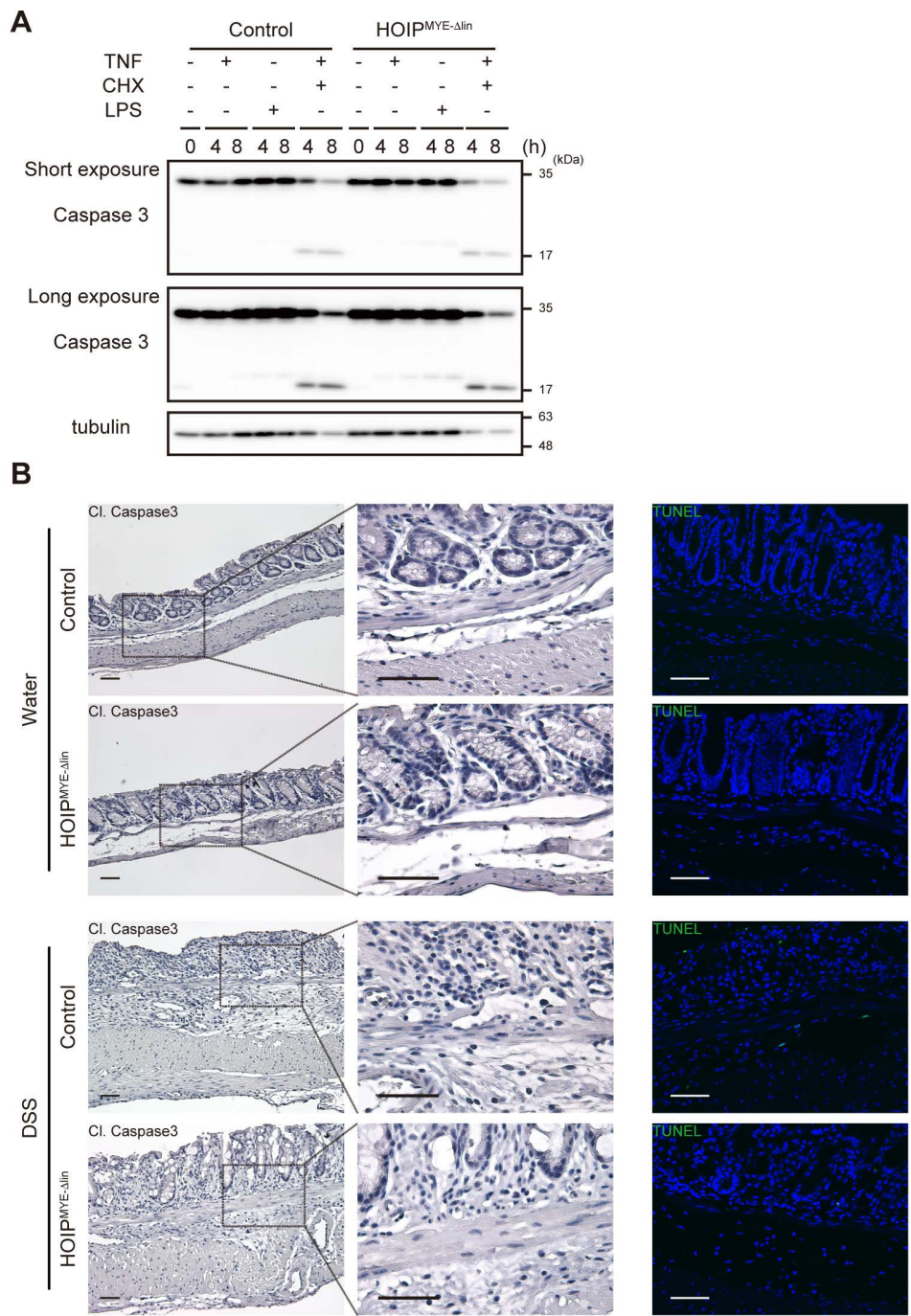


Figure S9

264

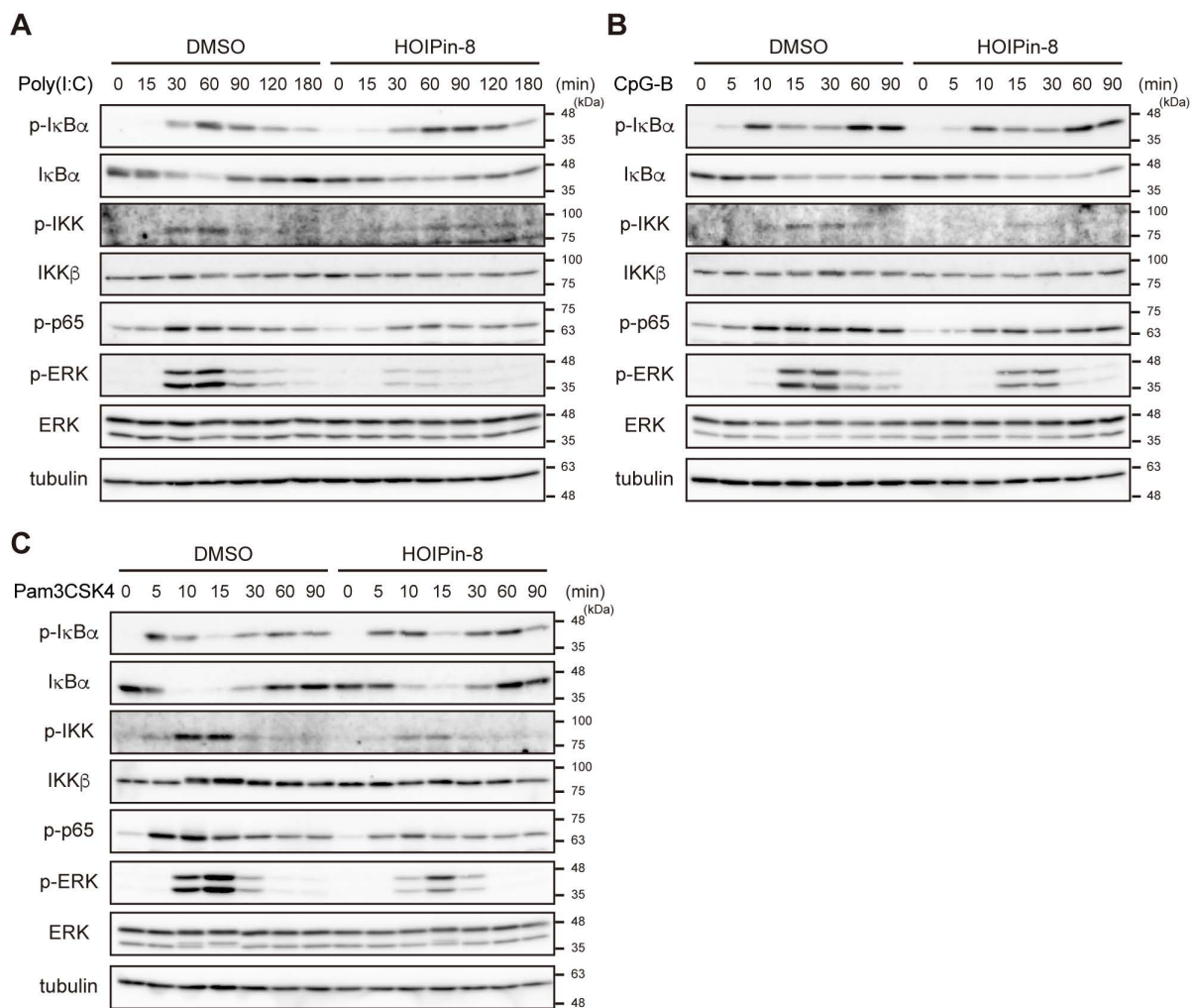
265 **Figure S9. Impaired linear ubiquitination activity in macrophages has no overt effect on**
 266 **cell death.**

267 (A) Immunoblot analysis of caspase 3 cleavage in BMDMs from control and HOIP^{MYE-Δlin}
 268 mice treated with TNF (10 ng/ml), LPS (10 ng/ml), or TNF (10 ng/ml) and CHX (20 μg/ml)
 269 for the indicated periods. Tubulin was used as a loading control. Data are representative of at

270 least two independent experiments.

271 (B) Immunohistochemical staining of the distal colon sections for cleaved caspase 3, and
272 immunofluorescence TUNEL staining, in control and HOIP^{MYE-Δlin} mice treated with DSS
273 (n=3). Data from untreated control and HOIP^{MYE-Δlin} mice are also shown (n=3). Scale bars,
274 50 μm.

275



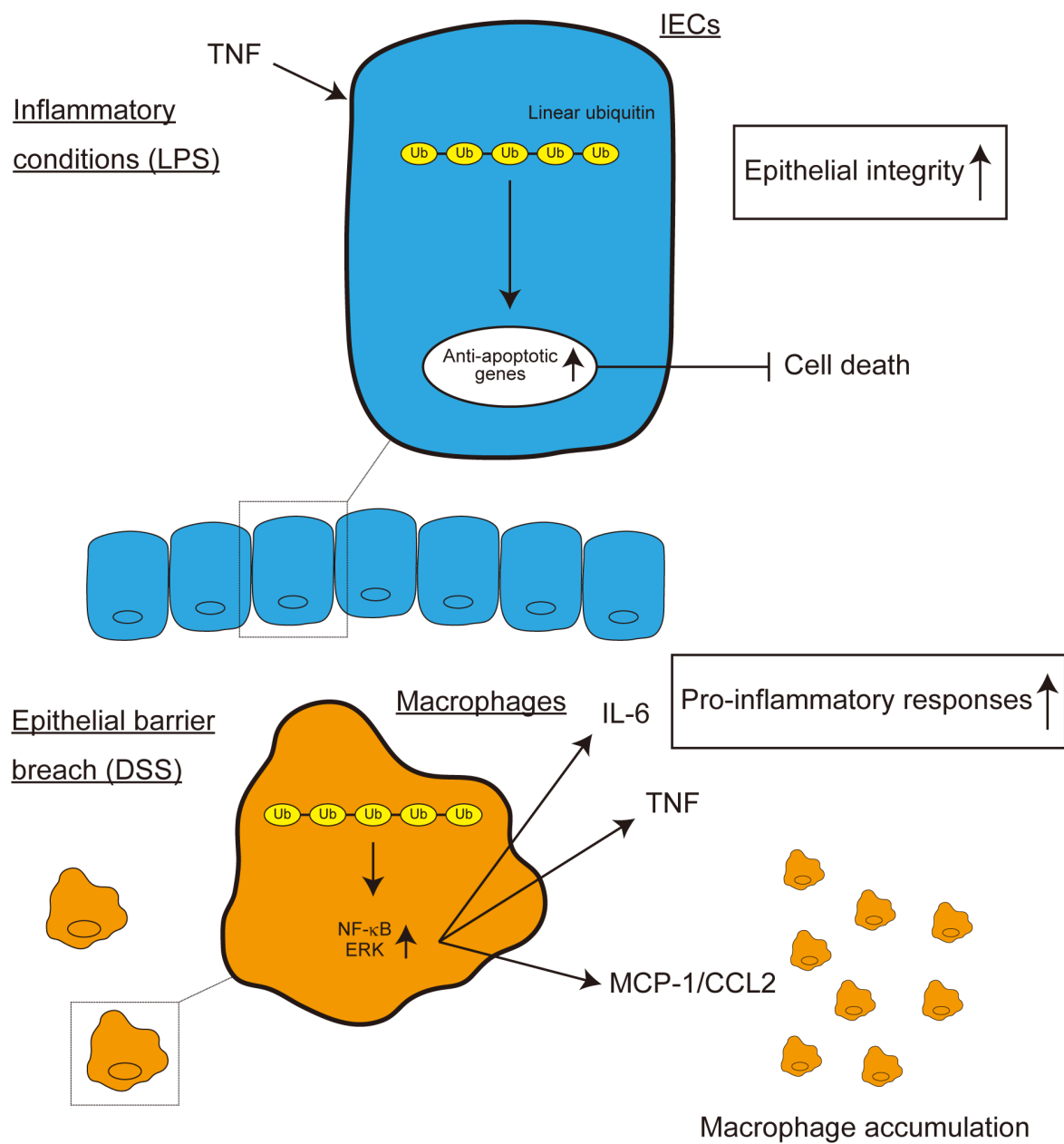
276

Figure S10

277 **Figure S10. Inhibiting LUBAC ligase activity impairs NF-κB and ERK activation upon**
278 **stimulation by multiple TLR ligands.**

279 (A, B, C) BMDMs from WT mice were pre-treated for 30 min with DMSO or HOIPin-8 (10
280 μM) and then stimulated with Poly(I:C) (2 μg/ml) (A), CpG-B (1 μM) (B), or Pam3CSK4 (1

281 $\mu\text{g/ml}$) (C) for the indicated times. Whole cell lysates were immunoblotted with the indicated
 282 antibodies. Tubulin was used as a loading control.
 283 A representative image of an immunoblot from at least two independent experiments is
 284 shown.
 285



286 **Figure S11**

287 **Figure S11. Schematic summarizing the different functions of linear ubiquitination in**

288 **IECs and macrophages.**

289 Under inflammatory conditions, linear ubiquitination in IECs regulates TNF-mediated
290 epithelial integrity by suppressing IEC death via up-regulation of anti-apoptotic genes. By
291 contrast, in the event of an epithelial barrier breach, linear ubiquitination in macrophages
292 regulates pro-inflammatory responses by producing pro-inflammatory cytokines (IL-6 and
293 TNF), and a chemokine that attracts macrophages (MCP-1/CCL2) downstream of activated
294 NF- κ B and ERK.

295

296 **Supplementary table legends**

297 **Table S1. List of primers used for qPCR analysis**

Table S1. List of primers used for qPCR analysis

Gene		Sequence
<i>Il1β</i>	Forward	5'-TGGACCTTCCAGGATGAGGACA-3'
	Reverse	5'-GTTTCATCTCGGAGCCTGTAGTG-3'
<i>Il6</i>	Forward	5'-TACCACTTCACAAGTCGGAGGC-3'
	Reverse	5'-CTGCAAGTGCATCATCGTTGTTC-3'
<i>Tnf</i>	Forward	5'-GGTGCCTATGTCTCAGCCTCTT-3'
	Reverse	5'-GCCATAGAAGTATGAGAGGGAG-3'
<i>Ccl2</i>	Forward	5'-CCGGCTGGAGCATCCACGTGT-3'
	Reverse	5'-TGGGGTCAGCACAGACCTCTCTCT-3'
<i>Cxcl1</i>	Forward	5'-TCCAGAGCTTGAAGGTGTTGCC-3'
	Reverse	5'-AACCAAGGGAGCTTCAGGGTCA-3'
<i>Cxcl2</i>	Forward	5'-CCAACCACCAGGCTACAGG-3'
	Reverse	5'-GCGTCACACTCAAGCTCTG-3'
<i>Birc3</i>	Forward	5'-GGACATTAGGAGTCTTCCCACAG-3'
	Reverse	5'-GAACACGATGGATACCTCTCGG-3'
<i>Tnfaip3</i>	Forward	5'-AGCAAGTGCAGGAAAGCTGGCT -3'
	Reverse	5'-GCTTTCGCAGAGGCAGTAACAG -3'
<i>Nfkbia</i>	Forward	5'-GCCAGGAATTGCTGAGGCACTT-3'
	Reverse	5'-GTCTGCGTCAAGACTGCTACAC-3'
<i>Lgr5</i>	Forward	5'-CCTACTCGAAGACTTACCCAGT-3'
	Reverse	5'-GCATTGGGGTGAATGATAGCA-3'
<i>Muc2</i>	Forward	5'-GGTCCAGGGTCTGGA TCACA-3'
	Reverse	5'-GCTCAGCTCACTGCCA TCTG-3'
<i>Alpi</i>	Forward	5'-TCCTACACCTCCATTCTCTATGG-3'
	Reverse	5'-CCGCCTGCTGCTTGTAG-3'
<i>Chga</i>	Forward	5'-ATCCTCTCTATCCTGCGACAC-3'
	Reverse	5'-GGGCTCTGGTTCTCAAACACT-3'
<i>Dclk1</i>	Forward	5'-TACCGACGCTATCAAGCTGGAC-3'
	Reverse	5'-GGTAACGGAAGTCTCTGGTCC-3'
<i>Lyz</i>	Forward	5'-TGACATCACTGCAGCCATAC-3'
	Reverse	5'-TGGGACAGATCTCGGTTTTG-3'
<i>Gapdh</i>	Forward	5'-TTCACCACCATGGAGAAGGC-3'
	Reverse	5'-GGCATGGACTGTGGTCATGA-3'